Full title

Diversity and functional specialization of oyster immune cells uncovered by integrative single cell level investigations

Short title

"Functional specialization in Oyster's immune cells"

Authors

Sébastien de La Forest Divonne[1], Juliette Pouzadoux[1], Océane Romatif[1], Caroline Montagnani[1], Guillaume Mitta[3], Delphine Destoumieux-Garzon[1], Benjamin Gourbal[2], Guillaume M. Charrière[1#], Emmanuel Vignal[1#*]

Affiliations

[1] IHPE, Univ Montpellier, CNRS, Ifremer, Univ Perpignan Via Domitia, Montpellier, France

[2] IHPE, Univ Montpellier, CNRS, Ifremer, Univ Perpignan Via Domitia, Perpignan, France

[3] Ifremer, IRD, Institut Louis-Malardé, Univ Polynésie française, UMR 241 SECOPOL, 98179 Taravao, Tahiti - Polynésie française, France

* corresponding author: emmanuel.vignal@umontpellier.fr

EV and GC co-supervised the work.

Abstract

Mollusks constitute a large part of the animal biodiversity and play an important role in ecosystems and global food security. The Pacific oyster, *Crassostrea (Magallana) gigas*, is the most farmed bivalve mollusc in the world and has become a model species. Despite the number of studies on bivalves' immune cells, the hemocytes, their characterization remains elusive. By using a combination of single-cell RNA sequencing, quantitative cytology, functional assays and trajectory analyses, we characterized a total of seven distinct hemocyte types and defined at least three hematopoietic lineages. This integrative analysis allowed us to reconcile molecular and cellular data and identify cell types performing specific immune functions such as phagocytosis,

ROS production, copper accumulation, and expression of antimicrobial peptides. These findings pave the way for a deeper understanding of key physiological and immune responses, to help develop mitigation strategies, limit the impact of disease and to contribute to the sustainability of bivalve farming.

Introduction

Mollusca is the second largest invertebrate phylum after Arthropoda, and the largest marine phylum, comprising approximately 23% of all known marine organisms (*1*)**.** Among them, bivalves are highly diverse and display a rich evolutionary history (*2*). The Pacific oyster *Crassostrea (Magallana) gigas* (*C. gigas* - Thunberg, 1793) (NCBI:txid29159) is a sessile filter-feeding bivalve that thrives in a variety of stressful environments ranging from intertidal to deep sea (*3*), and is key species for the aquaculture industry worldwide (*4*). Several infectious diseases affect *C. gigas* at different life stages, impacting its production, and considering its significant socio-economic value, considerable attention has been paid to better understand and to mitigate these diseases (*5*). The causes of these mortalities can involve a variety of pathogens, including viruses, bacteria and parasites that can be responsible for the mortality events affecting *C. gigas* (*6*). One of the most studied infectious diseases to date is the POMS (Pacific Oyster Mortality Syndrome), a polymicrobial disease responsible for mass mortalities of juvenile oysters (*7*). It is triggered by the OsHV-1 μVar herpesvirus, which alters the immune defenses of oysters and allows the colonization of opportunistic bacteria, including *Vibrio*, that cause hemocyte lysis and bacteremia that lead to animal death (*7*). Other bacterial pathogens have also been implicated in mass mortalities of adult Pacific oysters in several countries, and the most emblematic one is *Vibrio aestuarianus* which affects adults in Europe (*8*, *9*). To date, most of the oyster pathogens or opportunistic pathogens that have been characterized in detail have all been found to dampen hemocyte defenses during the pathogenic process, at their own benefit. These include the OsHV-1

51 μVar herpesvirus (*10*) and virulent *Vibrio* strains of the species *Vibrio crassostreae* and *Vibrio*
52 *tasmaniensis* (*11*), *Vibrio aestuarianus* and *Vibrio harveyi* (*12*), highlighting the critical role of
53 hemocytes in oyster immunity. Immune-based prophylactic treatments, such as immune-priming
54 and immune-shaping, have emerged as innovative solutions to enhance the natural defenses of
55 oysters against pathogens and increase their survival rate, but the development of such therapies is
56 still hampered by a limited knowledge of the underlying molecular and cellular mechanisms (*13*)
57 (*14*).

58 Hemocytes have been studied since the 1970s (for review see (*15*)). Hemocytes are known as
59 cellular effectors of the immune system that engage in phagocytosis to engulf and destroy
60 potential pathogens, neutralizing parasites by encapsulation, or preventing pathogen
61 dissemination by cell aggregation and release of extracellular DNA traps (*16*). They also
62 participate in the humoral response by releasing cytokines, antimicrobial peptides, and reactive
63 oxygen species (ROS) to combat the pathogens (*17*). In addition to their role in oyster immunity,
64 hemocytes have been implicated in numerous physiological processes ranging from shell repair
65 (*18*) to wound healing, nutrient transport, and environmental contaminant removal (*19*). Despite
66 this acquired knowledge, hemocytes represent a sum of under-characterized populations of
67 circulating immune cells, and knowledge of lineage ontogeny and functional specialization
68 remains poorly understood due to the lack of an unified classification and of limited molecular
69 and functional genetic tools. Several studies have proposed different classifications of hemocytes
70 in the *Ostreidae* family, with 3 to 4 hemocyte types reported (*15*), all based primarily on either
71 microscopic or flow cytometry analyses. In *C. gigas*, three primary hemocyte cell types have been
72 classically identified : blast, hyalinocyte, and granulocyte cells. While the immune response of *C.*
73 *gigas* has been extensively studied using classical transcriptomics either at the whole animal,
74 tissue or circulating hemocyte levels, these approaches have ignored the diversity of hemocyte
75 cell types and lineages underpinning these responses (*20*). However, accurately describing the

diversity of these cells, understanding their ontogeny, and delineating cell lineages is still a fundamental requirement for understanding their specific roles. Thanks to the emergence of single-cell RNA sequencing (scRNA-seq) techniques, it is now possible to monitor global gene expression at single-cell resolution with thousands of individual cells in a single experiment. This provides a unique opportunity to overcome these limitations and deepen our understanding of hemocyte diversity and function in bivalves. Recently scRNA-seq was used to provide a first molecular description of hemocyte population in the oyster *Crassotrea hongkongensis* (*21*). However, in the absence of morphological and/or functional characterization studies, the authors were unable to deduce the hemocyte cell types to be matched to the transcriptomic profiles generated by scRNA-seq.

While many transcriptomic analyses have been performed on *C. gigas* hemocytes, none have been performed at the single cell level. Here, we present an integrative study of *C. gigas* hemocyte diversity at the single cell level by combining scRNA-seq from a pathogen free adult oyster combined with cytology, cell fractionation and functional assays to provide a comprehensive transcriptomic, cytological and functional atlas of hemocyte cell types. Our scRNA-seq analyses identified 7 distinct transcriptomic populations and functional annotation revealed distinct populations with specific functions, including phagocytosis, oxidative burst, energetic metabolism, enhanced transcription, translation and cell division. Thanks to quantitative cytology, 7 morphologically distinct hemocyte cell types were identified, which allowed us to reconcile molecular and cytological data. Density gradients were used to separate hemocyte cell types and qPCR or functional assay analyses were performed to validate cell type-specific markers. Using this combination of analysis, we identified 1 type of hyalinocyte, 2 types of blasts and 4 types of granular cells. In addition, we determined cell types performing antimicrobial functions through phagocytosis, ROS production, copper accumulation, and expression of antimicrobial peptides. Finally, trajectory analysis of scRNA-seq data combined with functional analysis revealed distinct

differentiation pathways that may control hemocyte ontology and differentiation processes. Therefore, we propose here a deeper and up-to-date classification of *C. gigas* hemocytes with a more accurate description of the different cell types, their potential ontology and a precise description of their sub-functionalization.

Results

Single-cell RNA sequencing reveals 7 distinct transcriptomic clusters of circulating immune cells in oysters.

Oysters are known to express a high degree of individual genetic polymorphism, including Copy Number Variation (CNV) or the Presence Absence Variation (PAV) (*22*). Therefore, to avoid misinterpretation of the single-cell transcriptomic data, and to characterize the hemocyte cell types and their heterogeneity, we sampled hemocytes from a unique pathogen free animal (Ifremer Standardized Animal, 18 month-old) and applied single-cell drop-seq technology to 3,000 single hemocytes (**Fig. 1A**). The scRNA-seq library was generated and sequenced, resulting in 127,959,215 high-quality filtered reads available for single-cell analysis (ENA project accession number PRJEB74031). Primary bioinformatics was performed using the STAR solo aligner software (*23*) against the *C. gigas* genome (Genbank reference GCA_902806645.1) from the Roslin Institute (*24*). Out of 127,959,215 reads, 97% showed a valid barcode and 89.2% were mapped to the genome with a saturation of 75.6%. A total of 2,937 cells were profiled, yielding a median of 1,578 genes and 4,412 unique molecular identifiers (UMIs) per cell among the 23,841 total genes detected, with a sequencing saturation of 75.6% (**Supp. Table 1**). For secondary bioinformatic data processing, the Seurat R package (version 4.3.0) was used (*25*). To remove data corresponding to empty droplets or cell doublets, the data set was filtered. Cells with a gene number between 750 and 4,000 and with less than 5% mitochondrial genes were retained. After quality control processing 120 cells corresponding to empty droplets and cell doublets were removed and 2,817 cells were processed for data normalization. Finally, linear dimensional

126 reduction and clustering was performed on the 3,000 most variable genes from 2,817 cells (**Supp.**
127 **Fig. S1**). Dimension reduction and clustering led to the identification of 7 transcriptomic clusters
128 in which hemocytes were distributed. These 7 different clusters represented 27.6, 23.1, 17.8, 16.9,
129 7, 4.6 and 3% of the total cells (**Fig. 1B**). For each transcriptomic cluster, a pattern of over- and
130 under-represented transcripts in each cell was identified (**Fig. 1C**). Average Log2FC values and
131 percentage of expression in each cluster relative to all other clusters were calculated for the Top
132 10 differentially expressed genes (**Fig. 1D** and **Table 1)**. Clear transcriptomic cell clusters were
133 evidenced as well as specific gene markers for each cluster **(Supp. Data 1**). Only cluster 4
134 transcriptomic signature was less contrasting than that of other clusters (**Fig. 1D**).

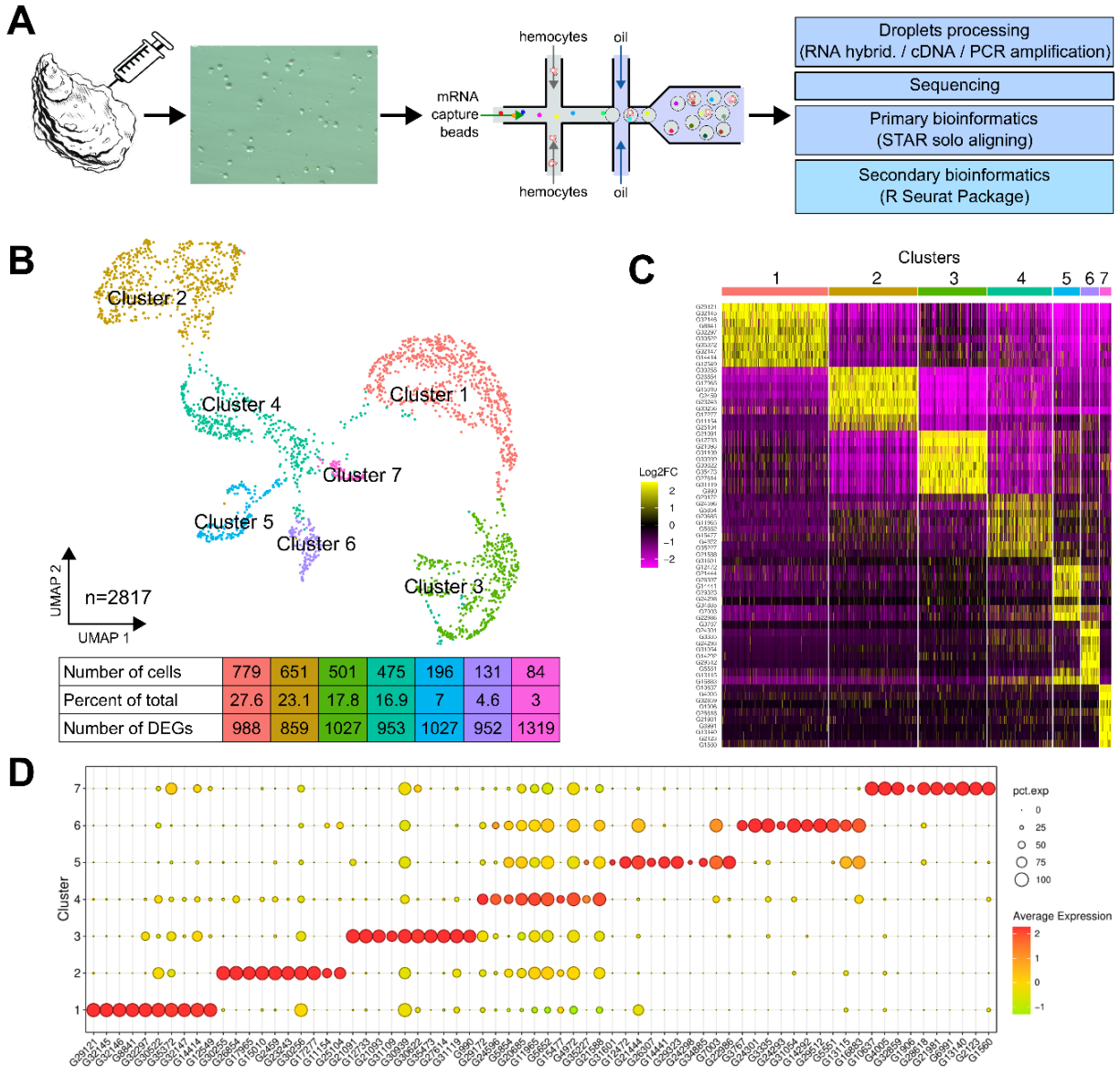

Number of cells	779	651	501	475	196	131	84
Percent of total	27.6	23.1	17.8	16.9	7	4.6	3
Number of DEGs	988	859	1027	953	1027	952	1319

Fig. 1. scRNA-seq analysis of *C. gigas* circulating hemocytes reveals 7 transcriptomic cell clusters (A) Schematic of the scRNA-seq 10X Genomics Chromium microfluidic technology and bioinformatics processing workflow used. Dissociated hemocytes were sampled from a pathogen-free oyster and encapsulated in droplets for processing. After sequencing, the data were processed bioinformatically. **(B)** Uniform Manifold Approximation and Projection (UMAP) plot for dimensional reduction of the data set and summary of the cells and the number of Differentially Expressed Genes (DEGs) in each cluster. The table displays the characteristics (number of cells, percentage of total cells and number of Differentially Expressed Genes in each cluster) of the seven clusters identified. **(C)** Heatmap showing the top 10 overexpressed genes in each cell per

145 cluster as determined by *FindAllMarkers()* function in Seurat, corresponding to clusters in UMAP
146 plots from **Fig. 1B**, ranked by log2FC. **(D)** Dot plot representing the top ten DEGs enriched per
147 cluster based on average expression (avg_log2FC). Color gradient of the dot represents the
148 expression level, while the size represents the percentage of cells expressing any gene per cluster.

Gene	log2FC	Pct 1	Pct 2	Description
				Cluster 1
G29121	4.31	1	0.099	L-galactono-gamma-lactone oxidase
G32145	4.18	0.992	0.079	Angiopoietin-1 receptor
G32146	3.90	0.985	0.063	Angiopoietin-1 receptor
G8841	3.13	0.988	0.049	C-type lectin domain-containing protein
G32297	2.88	0.99	0.232	PNPLA domain-containing protein
G30522	2.76	1	0.515	Cytochrome P450 2D28
G35372	2.69	1	0.483	60S ribosomal protein L26
G32147	2.45	0.969	0.131	Angiopoietin-1 receptor
G14414	2.45	1	0.343	DUF4773 domain-containing protein
G12549	2.38	0.974	0.132	Glutaredoxin domain-containing protein
				Cluster 2
G30255	5.31	1	0.15	Metalloproteinase inhibitor 3
G26854	4.24	1	0.16	Stanniocalcin
G17965	4.21	0.94	0.04	Complement C1q-like protein 2
G15010	3.99	0.99	0.17	Kyphoscoliosis peptidase
G2459	3.82	1	0.21	*Uncharacterized protein*
G23243	3.51	0.98	0.07	Fibronectin type-III domain-containing protein
G30256	3.23	1	0.69	NTR domain-containing protein
G17277	3.21	0.99	0.04	Putative modulator of levamisole receptor-1
G11154	3.16	0.68	0.05	Collagen alpha-1(XII) chain
G25104	3.1	0.84	0.08	C1q domain-containing protein
				Cluster 3
G21091	5.51	0.99	0.13	X-box binding protein-like protein
G12733	5.42	1	0.12	Galectin
G21093	5.17	0.94	0.05	IoIG
G31109	4.36	0.77	0.03	Cystatin domain-containing protein
G30939	4.25	1	0.86	Peptide ABC transporter permease
G30622	3.95	1	0.21	BHLH domain-containing protein
G35473	3.86	0.96	0.04	*Uncharacterized protein*
G27614	3.78	0.96	0.13	G Protein Receptor F1-2 domain-containing protein
G31119	3.77	0.99	0.42	Arrestin C domain-containing protein
G990	3.6	0.93	0.03	LITAF domain-containing protein
				Cluster 4
G29172	3.09	0.78	0.49	G Protein Receptor F1-2 domain-containing protein
G24596	2.37	0.78	0.25	High mobility group protein DSP1
G5854	1.8	0.64	0.38	N-acetyltransferase domain-containing protein
G20685	1.59	0.88	0.53	Ribosomal protein L22
G11965	1.57	0.92	0.7	Ribosome L4 associated C domain-containing protein
G5652	1.54	0.97	0.75	60S ribosomal protein L30
G15477	1.52	0.55	0.3	Metalloendopeptidase
G4972	1.49	0.96	0.8	60S ribosomal protein L12
G35227	1.46	0.55	0.06	ML domain-containing protein
G21588	1.42	0.94	0.69	60S ribosomal protein L13

Gene	log2FC	Pct 1	Pct 2	Description
				Cluster 5
G31601	5.24	0.38	0.06	Polyribonucleotide nucleotidyltransferase
G12472	3.99	0.85	0.03	Galectin
G21444	3.58	1	0.41	*Uncharacterized protein*
G26307	3.42	0.6	0.02	*Uncharacterized protein*
G14441	3.35	0.84	0.08	CUBN
G29323	3.21	0.9	0.01	GTPase IMAP family member 4
G24298	3.18	0.29	0.05	Putative Transmembrane protease serine 9
G34885	3.13	0.59	0.01	Gliding motility-associated C-terminal domain-containing protein
G7003	2.55	0.99	0.16	ETS-related transcription factor Elf-4
G22986	2.37	0.94	0.1	Metalloendopeptidase
				Cluster 6
G3767	6.45	0.74	0.02	Natterin-1
G24301	6.16	0.99	0.02	Aspartate-semialdehyde dehydrogenase
G3335	5.19	1	0.16	*ncRNA*
G24293	4.57	0.59	0.01	*Uncharacterized protein*
G31054	3.56	1	0.13	GATA-binding factor 3
G14292	3.29	0.87	0.03	Membrane-associated guanylate kinase inverted 3
G29512	3.2	0.99	0	Caveolin
G5551	2.93	0.97	0.02	Neuronal acetylcholine receptor subunit alpha-6
G13115	2.73	0.83	0.26	*ncRNA*
G16883	2.62	1	0.2	Allograft inflammatory factor
				Cluster 7
G10637	4.21	0.99	0.03	BZIP domain-containing protein
G4005	4.07	0.99	0.21	Ras-related protein Rab-20
G32859	3.9	0.93	0.04	G Protein Receptor F1-2 domain-containing protein
G1906	3.82	0.5	0.02	Glutathione peroxidase
G28618	3.53	0.91	0.09	Sporozoite and liver stage asparagine-rich protein
G21981	3.5	0.94	0.05	*ncRNA*
G6991	3.4	0.85	0.01	Rho-GAP domain-containing protein
G13140	3.12	1	0.03	DBH-like monooxygenase protein 1
G2123	3.05	0.94	0.02	SPRY domain-containing SOCS box protein 3
G1560	3.02	0.95	0.17	Glutathione peroxidase

149

150 **Table 1. Top 10 overexpressed genes identified in each transcriptomic cluster.** The first
151 column gives the gene number according to the annotation. 'log2FC' represents the log2 fold
152 change of the gene in the cluster compared to all other cells. 'Pct1' is the percentage of cells
153 expressing the gene in the cluster and 'Pct2' is the fraction of cells expressing the gene in all other
154 clusters. Description is the annotation of the expressed gene.

155

156 **KEGG pathways and GO-terms analyses unveil functional diversity in *C. gigas* hemocytes**

157 ScRNA-seq data evidenced specific functions carried by hemocyte cell types composing the
158 seven transcriptomic clusters. A first global view of the functions over-represented in each cluster

159 was obtained through a KEGG pathway analysis on the overrepresented transcripts (Log2FC >
160 0.25) using the *C. gigas* annotation provided by the DAVID consortium (*26*), thereby identifying
161 pathways specifically enriched in each cluster. Cluster 1 was enriched in viral processing and
162 endocytosis (**Figure 2A** and **Supplemental Table S2**). It was also enriched in pyruvate
163 metabolism, glycolysis/gluconeogenesis and pentose phosphate pathways. Clusters 1 and 3
164 showed a specific enrichment in carbohydrate metabolism and endocytosis. Particularly, cluster 3
165 was enriched transcripts implicated in glycolysis/gluconeogenesis and TCA cycle activities.
166 Cluster 4 was enriched in protein synthesis, including transcription (spliceosome, ribosome,
167 nucleocytoplasmic transport and mRNA surveillance pathway) folding, sorting and degradation of
168 protein pathways. Clusters 2, 5 and 6 shared a common signature of enrichment in ribosome-
169 related genes, while cluster 2 was specifically enriched in motor protein-coding genes responsible
170 for cell motility and xenobiotic metabolism. Remarkably, clusters 1, 3, 4 and 5 were enriched in
171 oxidative phosphorylation transcripts, whereas cluster 7 was enriched in vesicular trafficking and
172 endo-lysosomal pathways (endocytosis, endosome, phagosome, lysosome, auto and mitophagy).

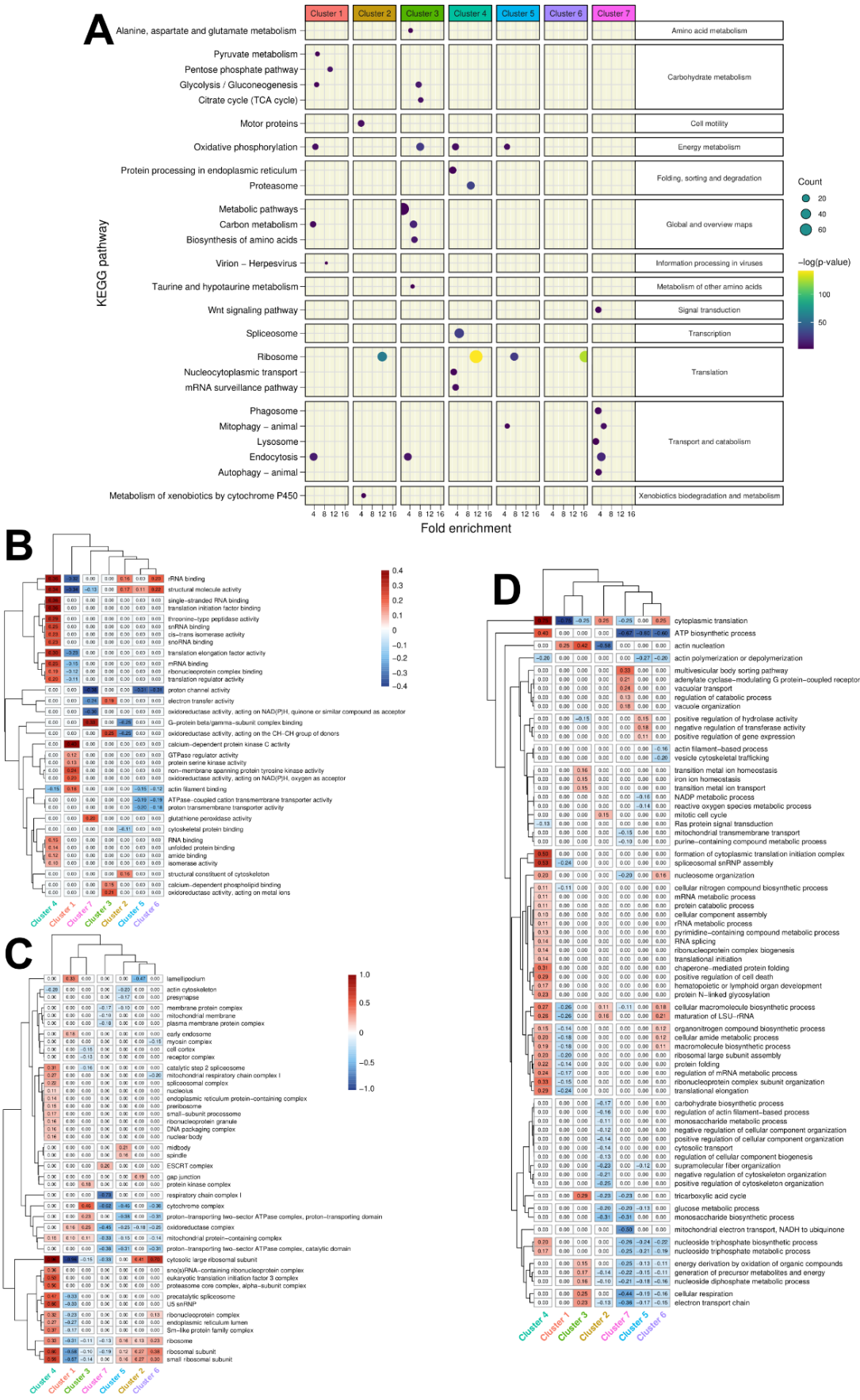
A
Cluster 1
Cluster 2
Cluster 3
Cluster 4
Cluster 5
Cluster 6
Cluster 7
KEGG pathway
Alanine, aspartate and glutamate metabolism
Pyruvate metabolism
Pentose phosphate pathway
Glycolysis / Gluconeogenesis
Citrate cycle (TCA cycle)
Motor proteins
Oxidative phosphorylation
Protein processing in endoplasmic reticulum
Proteasome
Metabolic pathways
Carbon metabolism
Biosynthesis of amino acids
Virion – Herpesvirus
Taurine and hypotaurine metabolism
Wnt signaling pathway
Spliceosome
Ribosome
Nucleocytoplasmic transport
mRNA surveillance pathway
Phagosome
Mitophagy – animal
Lysosome
Endocytosis
Autophagy – animal
Metabolism of xenobiotics by cytochrome P450
Amino acid metabolism
Carbohydrate metabolism
Cell motility
Energy metabolism
Folding, sorting and degradation
Global and overview maps
Information processing in viruses
Metabolism of other amino acids
Signal transduction
Transcription
Translation
Transport and catabolism
Xenobiotics biodegradation and metabolism
Count
20
40
60
−log(p-value)
100
50
Fold enrichment
B
rRNA binding
structural molecule activity
single−stranded RNA binding
translation initiation factor binding
threonine−type peptidase activity
snRNA binding
cis−trans isomerase activity
snoRNA binding
translation elongation factor activity
mRNA binding
ribonucleoprotein complex binding
translation regulator activity
proton channel activity
electron transfer activity
oxidoreductase activity, acting on NAD(P)H, quinone or similar compound as acceptor
G−protein beta/gamma−subunit complex binding
oxidoreductase activity, acting on the CH−CH group of donors
calcium−dependent protein kinase C activity
GTPase regulator activity
protein serine kinase activity
non−membrane spanning protein tyrosine kinase activity
oxidoreductase activity, acting on NAD(P)H, oxygen as acceptor
actin filament binding
ATPase−coupled cation transmembrane transporter activity
proton transmembrane transporter activity
glutathione peroxidase activity
cytoskeletal protein binding
RNA binding
unfolded protein binding
amide binding
isomerase activity
structural constituent of cytoskeleton
calcium−dependent phospholipid binding
oxidoreductase activity, acting on metal ions
Cluster 4
Cluster 1
Cluster 7
Cluster 3
Cluster 2
Cluster 5
Cluster 6
C
lamellipodium
actin cytoskeleton
presynapse
membrane protein complex
mitochondrial membrane
plasma membrane protein complex
early endosome
myosin complex
cell cortex
receptor complex
catalytic step 2 spliceosome
mitochondrial respiratory chain complex I
spliceosomal complex
nucleolus
endoplasmic reticulum protein−containing complex
preribosome
small−subunit processome
ribonucleoprotein granule
DNA packaging complex
nuclear body
midbody
spindle
ESCRT complex
gap junction
protein kinase complex
respiratory chain complex I
cytochrome complex
proton−transporting two−sector ATPase complex, proton−transporting domain
oxidoreductase complex
mitochondrial protein−containing complex
proton−transporting two−sector ATPase complex, catalytic domain
cytosolic large ribosomal subunit
sno(s)RNA−containing ribonucleoprotein complex
eukaryotic translation initiation factor 3 complex
proteasome core complex, alpha−subunit complex
precatalytic spliceosome
U5 snRNP
ribonucleoprotein complex
endoplasmic reticulum lumen
Sm−like protein family complex
ribosome
ribosomal subunit
small ribosomal subunit
Cluster 4
Cluster 1
Cluster 3
Cluster 7
Cluster 5
Cluster 2
Cluster 6
D
cytoplasmic translation
ATP biosynthetic process
actin nucleation
actin polymerization or depolymerization
multivesicular body sorting pathway
adenylate cyclase−modulating G protein−coupled receptor signaling pathway
vacuolar transport
regulation of catabolic process
vacuole organization
positive regulation of hydrolase activity
negative regulation of transferase activity
positive regulation of gene expression
actin filament−based process
vesicle cytoskeletal trafficking
transition metal ion homeostasis
iron ion homeostasis
transition metal ion transport
NADP metabolic process
reactive oxygen species metabolic process
mitotic cell cycle
Ras protein signal transduction
mitochondrial transmembrane transport
purine−containing compound metabolic process
formation of cytoplasmic translation initiation complex
spliceosomal snRNP assembly
nucleosome organization
cellular nitrogen compound biosynthetic process
mRNA metabolic process
protein catabolic process
cellular component assembly
rRNA metabolic process
pyrimidine−containing compound metabolic process
RNA splicing
ribonucleoprotein complex biogenesis
translational initiation
chaperone−mediated protein folding
positive regulation of cell death
hematopoietic or lymphoid organ development
protein N−linked glycosylation
cellular macromolecule biosynthetic process
maturation of LSU−rRNA
organonitrogen compound biosynthetic process
cellular amide metabolic process
macromolecule biosynthetic process
ribosomal large subunit assembly
protein folding
regulation of mRNA metabolic process
ribonucleoprotein complex subunit organization
translational elongation
carbohydrate biosynthetic process
regulation of actin filament−based process
monosaccharide metabolic process
negative regulation of cellular component organization
positive regulation of cellular component organization
cytosolic transport
regulation of cellular component biogenesis
supramolecular fiber organization
negative regulation of cytoskeleton organization
positive regulation of cytoskeleton organization
tricarboxylic acid cycle
glucose metabolic process
monosaccharide biosynthetic process
mitochondrial electron transport, NADH to ubiquinone
nucleoside triphosphate biosynthetic process
nucleoside triphosphate metabolic process
energy derivation by oxidation of organic compounds
generation of precursor metabolites and energy
nucleoside diphosphate metabolic process
cellular respiration
electron transport chain
Cluster 4
Cluster 1
Cluster 3
Cluster 2
Cluster 7
Cluster 5
Cluster 6

174 **Fig. 2. KEGG and Gene Ontology analysis of the gene signature in each cluster. (A)** A
175 synthetic representation of the KEGG pathway analysis is shown. Colored columns represent the
176 7 transcriptomic clusters. Each row is a KEGG pathway, the colored dot represents the -log(p-
177 value) and the dot size represents the number (count) of enriched genes in each pathway category.
178 The fold enrichment is shown on the x-axis. Panels **(B), (C)** and **(D)** show the results of Gene
179 Ontology terms (GO-terms) for Biological Processes (BP), Cellular Components (CC) and
180 Molecular Functions (MF) respectively, obtained with the overexpressed genes of each cluster
181 (Absolute value Log2FC > 0.25 and significant p-value < 0.001) using RBGOA analysis (p-value
182 <= 0.001) for three different ontology universes. Each panel corresponds to one ontology
183 universe, and the analysis highlights over- and under-enriched terms. The number in the heatmap
184 and the scale indicate the proportion of significant positive GO-terms. Positive values indicate
185 over-enrichment and negative values indicate under-enrichment of the respective BP, CC and MF
186 ontologies.

187 To delve deeper into the functional characterization of each transcriptomic cluster, we performed
188 a re-annotation of the *C. gigas* genome using a combination of tools to increase the GO term
189 richness of the current annotation prior to functional GO term analysis. For this purpose, we used
190 the *C. gigas* genome (Genbank reference GCA_902806645.1) and the associated gff3 annotation
191 file from the Roslin Institute (*27*). Using these files, the longest CDSs were extracted and
192 processed for GO-term annotation using the Orson pipeline (see Materials and methods). Of the
193 30,724 CDSs extracted, 22,462 CDSs were annotated (GO-terms and sequence description),
194 resulting in an annotation percentage of 73.1%. Of the 30,724 CDSs, 22,391 were annotated with
195 Molecular Functions (MF), Biological Processes (BP), and Cellular Components (CC) GO-terms
196 (**Supp. Fig. S2 and Supp. Data 2**). Using the GO-term annotation and the Log2FC of genes
197 calculated after scRNA-seq processing in each cluster, GO enrichment analysis was performed by

198 a rank-based gene ontology analysis (RBGOA) (*28*). RBGOA analysis was performed on GO-
199 terms identified in each cluster (**Supp. Data 3**). Results are shown in **Figures 2B, C and D**.
200
201 Overall, scRNA-seq-based analysis identified seven distinct transcriptomic profiles for each cell
202 cluster, shedding light on greater heterogeneity and functional diversity of *C. gigas* hemocytes
203 than previously described. Cluster 1, encompassing 27.6 % of cells, is characterized by
204 morphology and actin cytoskeleton remodeling capacity and oxidoreductase activity, as indicated
205 by an enrichment in oxidoreductase activity acting on NAD(P)H and kinase activities BP, actin
206 nucleation MF and lamellipodium and early endosomes CC. Cluster 2, comprising 23.1 % of
207 cells, has an increased translation activity, as indicated by enrichment in BP, MF and CC terms
208 related to rRNA binding, cytoplasmic translation, maturation of LSU-rRNA, and ribosomes
209 respectively. Cluster 3, making up 17.8 % of cells, shows enrichment in cellular oxidation and
210 actin nucleation, as indicated by an enrichment in BP and MF related to oxidoreductase activities
211 acting on metal ions, electron transfer, cellular oxidation and actin nucleation, and CC related to
212 cytochromes, oxidoreductase complex, and mitochondrial protein-containing complexes. Cluster
213 4, include 16.9 % of the cells, has transcriptomic signatures reminiscent of spliceosome assembly,
214 rRNA maturation, and ATP biosynthesis (BP related to RNA binding, translation, and
215 proteasome, MF related to spliceosome assembly, rRNA maturation, and ATP biosynthesis, and
216 CC related to nuclear bodies and ribosomes). Cluster 5, with 7 % of cells, shows enrichment in
217 structural molecule activity, hydrolase regulation, and gene expression, evident in its BP, MF, and
218 CC related to ribosome, midbody and spindle localization. Cluster 6, comprising 4.6 % of cells,
219 is characterized by nucleosome organization, translation, and biosynthetic processes, with related
220 BP, MF, and CC tied to ribosomes, ribonucleoprotein complex and rRNA binding. Cluster 7,
221 representing 3 % of cells only, is characterized by multivesicular body sorting, vacuolar transport,

222 vacuole organization, and G protein-coupled receptor signaling, with related BP, MF, and CC of
223 the ESCRT machinery.

224 **Seven morphologically distinct immune cell types are identified by quantitative cytology**
225 **and transcriptomic markers.**

226 To better characterize the diversity of circulating hemocytes in *C. gigas*, cytological studies were
227 performed using MCDH staining.

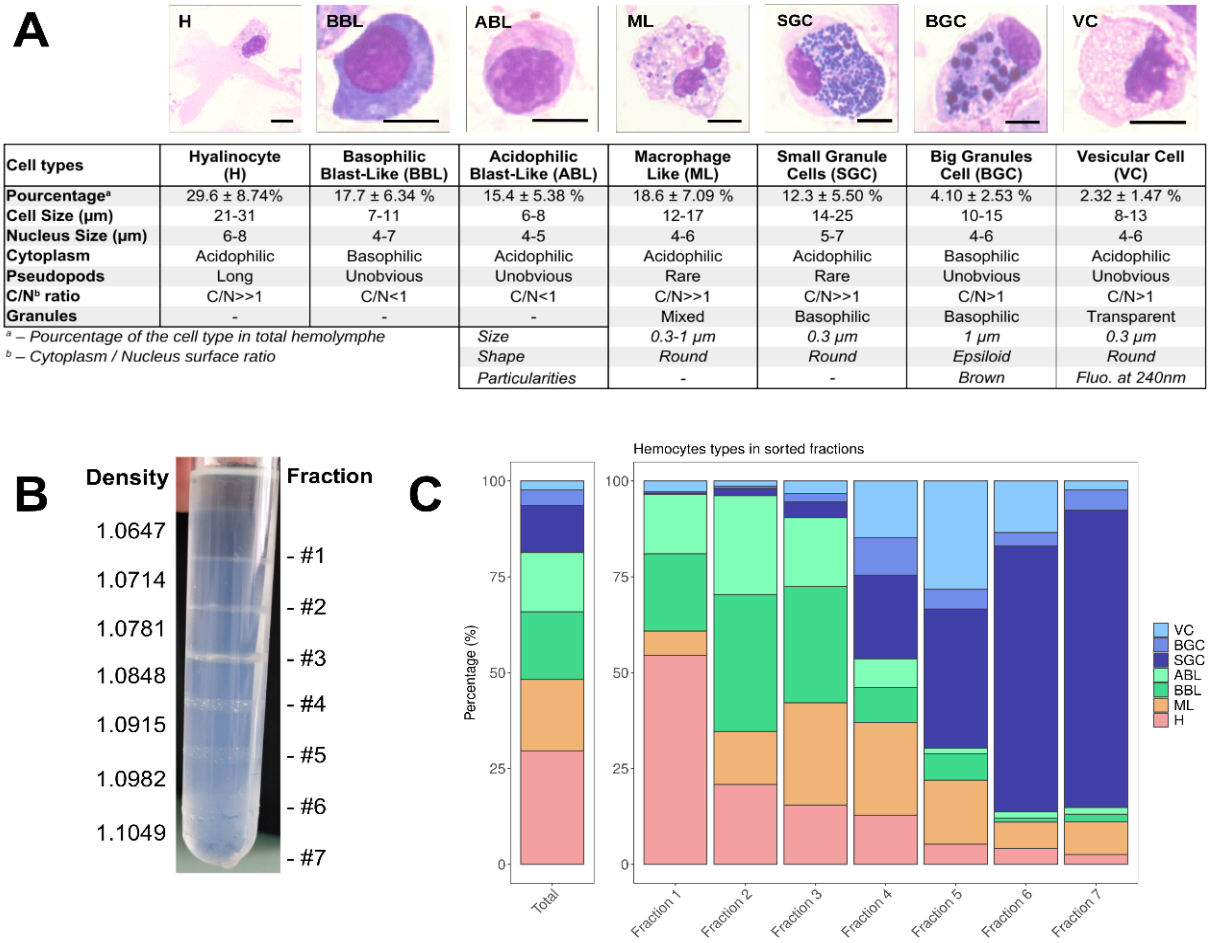

Cell types	Hyalinocyte (H)	Basophilic Blast-Like (BBL)	Acidophilic Blast-Like (ABL)	Macrophage Like (ML)	Small Granule Cells (SGC)	Big Granules Cell (BGC)	Vesicular Cell (VC)
Pourcentage[a]	29.6 ± 8.74%	17.7 ± 6.34 %	15.4 ± 5.38 %	18.6 ± 7.09 %	12.3 ± 5.50 %	4.10 ± 2.53 %	2.32 ± 1.47 %
Cell Size (µm)	21-31	7-11	6-8	12-17	14-25	10-15	8-13
Nucleus Size (µm)	6-8	4-7	4-5	4-6	5-7	4-6	4-6
Cytoplasm	Acidophilic	Basophilic	Acidophilic	Acidophilic	Acidophilic	Basophilic	Acidophilic
Pseudopods	Long	Unobvious	Unobvious	Rare	Rare	Unobvious	Unobvious
C/N[b] ratio	C/N>>1	C/N<1	C/N<1	C/N>>1	C/N>>1	C/N>1	C/N>1
Granules	-	-	-	Mixed	Basophilic	Basophilic	Transparent
			Size	*0.3-1 µm*	*0.3 µm*	*1 µm*	*0.3 µm*
			Shape	*Round*	*Round*	*Epsiloid*	*Round*
			Particularities	-	-	*Brown*	*Fluo. at 240nm*

[a] – Pourcentage of the cell type in total hemolymphe
[b] – Cytoplasm / Nucleus surface ratio

228

229 **Fig 3. *C. gigas* naive hemocyte formula and Percoll gradient hemolymph fractionation (A)**
230 Morphology, percentages and characteristics of the 7 cell types identified by MCDH staining. **H** :
231 Hyalinocyte, **ML** : Macrophage Like, **BBL** : Basophilic Blast Like cell, **ABL** : Acidophilic Blast
232 Like cell, **SGC** : Small Granule Cell, **BGC** : Big Granule Cell, **VC** : Vesicular Cell. Scale bar : 5
233 µm. Hyalinocytes (54%) and blast cells (ABL & BBL) (35%) were predominant in the first
234 fraction. The second fraction saw an increase in blasts (ABL 26%, BBL 36%) and a decrease in

235 hyalinocytes (21%). Fraction 3 had a mixed content with a decrease in hyalinocytes and blasts
236 (15%), and majority being blasts and macrophage-like cells. Fraction 4 had an increase in
237 granular cells (SGC 22%, BGC 10%, VC 15%) and a decrease in blasts (ABL 8%, BBL 9%).
238 Fraction 5 showed an increase in small granule cells (36%) and vesicular cells (28%), and a
239 decrease in big granule cells (5%). Fraction 6 had fewer hyalinocytes, macrophage-like, and blast
240 cells compared to small granule cells and vesicular cells. The last fraction was mainly small
241 granule cells (81%). **(B)** Hemocyte sorting on a discontinuous Percoll gradient. 7 fractions were
242 identified along the gradient at the top of each density cushion (from d=1.0647 at #1 to d= 1.1049
243 at #7). **(C)** Representation of the average values (from 5 different fractionation experiments) of
244 the different hemocyte types in the seven percoll gradient fractions compared to an average
245 hemolymph composition of a naive oyster (Total). **VC** : Vesicular Cells, **BGC** : Big Granule
246 Cells, **SGC** : Small Granule Cells, **ABL** : Acidophilic Blast Like cells, **BBL** : Basophilic Blast
247 Like cells, **ML** : Macrophage Like cells and **H** : Hyalinocytes respectively. (**Supp. Fig. S4** for
248 statistics).

249

250 We were able to define seven different hemocyte morphotypes : 3 non-granular (acidophilic
251 blasts, basophilic blasts and hyalinocytes) and 4 granular (small granule cells, big granule cells,
252 vesicular cells and macrophage-like) **(Fig. 3 and Supp. Fig. S3)**. Hyalinocytes (30% of total
253 hemocytes) are large cells with an irregular spreading membrane, containing an azurophilic
254 cytoplasm without granulations, the nucleus is irregular and varies in size (**Fig. 3A panel H**).
255 Macrophage-like cells (19% of the hemocytes) present an irregular membrane punctuated by rare
256 pseudopodia with a polylobed nucleus and a basophilic cytoplasm where polychromatic
257 inclusions of various sizes could be observed (**Fig 3A. panel ML**). Basophilic blasts
258 characterized by a basophil cytoplasm (**Fig. 3A panel BBL**) and acidophilic blasts with acidophil
259 cytoplasm (**Fig. 3A panel ABL**) accounted for 18% and 15% of the total hemocytes respectively.

260 They are rounded cells without granulation with an uniform and regular dense nucleus and a high
261 nucleo-cytoplasmic ratio. Small granule cells, (12% of the total hemocytes) have an irregular
262 membrane punctuated by rare pseudopodia, an acidophilic cytoplasm, and numerous
263 homogeneous purple granules (**Fig. 3A panel SGC**). Big granule cells (4% of the total
264 hemocytes) are rounded cells with a basophilic cytoplasm containing large, slightly dark purple to
265 black vesicles of heterogeneous size (**Fig. 3A panel BGC**). Vesicular cells representing 2% of
266 the hemocytes, are rounded cells with acidophilic cytoplasm, rich in homogeneous transparent
267 and fluorescent to UV light vesicles with an irregular nucleus (**Fig. 3A panel VC**). Only blasts
268 (BBL, ABL) show a nucleo-cytoplasmic ratio less than 1, whereas the other hemocytes described
269 show a nucleo-cytoplasmic ratio greater than 1.
270 To go further in the functional characterization of these diverse hemocyte morphotypes and to
271 associate them with the transcriptomic clusters identified in the scRNA-seq, we improved a
272 hemocyte fractionation approach using an isopycnic Percoll density gradient to sort the
273 hemocytes (*29*). Cell sorting was performed using a discontinuous Percoll gradient with densities
274 ranging from 1.0647 to 1.1049. Seven different density fractions were constituted (**Fig. 3B**) and
275 hemocyte composition was then characterized by cytology visualization from each fraction (**Fig.
276 3A;** see also **Supp. Fig. S4** for statistical significance). Hemocyte morphotypes were unevenly
277 distributed along the density gradient allowing a relative separation of the different cell
278 populations (**Supp. Fig S4**). To summarize, hyalinocytes were significantly enriched in the first
279 fraction, macrophage-like cells were significantly enriched in fraction 3 and in fraction 4.
280 Acidophilic blasts were significantly enriched in fractions 2. Basophilic blasts were significantly
281 enriched in fractions 2 and 3. Vesicular cells were enriched in fraction 5, big granule cells were
282 enriched in the fraction 4 and small granule cells in fraction 6 and 7 (**Fig. 3C and Supp. Fig. S4**).

283 In order to identify the transcriptomic cell clusters corresponding to the different hemocyte
284 morphotypes we used a RT-qPCR to detect the expression of different cluster-specific marker

genes in the different hemocytes in the Percoll density fractions. Marker genes were selected without a priori based only on their expression levels (Log2FC) and on their percentage of expression (Pct1 / Pct2 ratio) in the cluster of interest relative to all other cell clusters (**Table 2).** The expression level of each marker in the seven different clusters confirmed that the 14 selected marker genes were differentially expressed in each scRNA-seq transcriptomic cluster (**Supp. Fig. S5**).

Gene Number	Avg. Log2FC	Pct.1/Pct.2 Ratio	Cluster	Description	Marker Name
G8994	2.05	38.20	1	Laccase-24	LACC24
G8841	3.13	20.16		C-type lectin domain-containing protein	CLEC
G24846	2.31	31.52	2	EGF-like domain-containing protein 8	EGFL
G17277	3.21	23.00		Putative modulator of levamisole receptor-1	LEVAR
G22387	3.16	16.76	3	TGc domain-containing protein	TGC
G21091	5.51	7.69		X-box binding protein-like protein	XBOX
G35227	1.46	9.98	4	ML domain-containing protein	MLDP
G31074	0.94	6.51		High mobility group protein B1	HMGB1
G14441	3.35	11.01	5	Cubilin	CUBN
G12472	3.99	24.91		Galectin	GAL
G29512	3.20	246.25	6	Caveolin	CAV
G3767	6.45	41.11		Natterin-1	NAT1
G13140	3.12	40.00	7	DBH-like monooxygenase protein 1	MOX
G32859	3.90	23.82		G protein receptor F1-2 domain-containing protein	GPROT

Table 2. Table of the 14 marker genes specific to the different transcriptomic clusters. Gene number, average Log2FC, pct1/pct2 ratio (percentage of cells expressing this transcript in the cluster divided by the percentage of all other cells expressing this transcript) and cluster number are reported. The description is taken from our annotation and the marker name was derived from the description.

RT-qPCR expression profiles in the hemocyte fractions obtained from Percoll density gradient revealed distinct patterns according to the different transcriptomic cluster marker genes (**Fig. 4A**). Cluster 1 markers (LACC24 and CLEC) were overexpressed in fractions 1, 2, 3 and underexpressed in the other fractions relative to the total hemocytes. Cluster 2 markers (EGFL and LEVAR) showed a decreasing pattern of expression from fraction 1 to fraction 7. Cluster 3

303 markers (TGC and XBOX) showed significant increase in expression in fraction 4 to 7. Cluster 4
304 markers (MLDP and HMGB1) showed a gradually decreasing expression pattern from fraction 2
305 to fraction 7. Cluster 5 marker genes (GAL and CUBN) were underexpressed in fractions 4 to 7,
306 but not differentially expressed in fractions 1 to 3 compared to total hemocytes. Cluster 6 marker
307 genes (CAV and NAT1) were overexpressed in fraction 3, expressed similarly to total hemocytes
308 in fraction 2, and underexpressed in fractions 1, and 4 to 7. Finally, cluster 7 marker genes (MOX
309 and GPROT) were overexpressed only in fractions 3 to 7. A clear association between hemocyte
310 morphotypes and 14 gene markers could be evidenced by correlation analysis and statistical
311 validation (**Fig. 4B, Fig. 4C and Supp. Table S4**). Cluster 3 marker genes (TGC and XBOX)
312 correlated positively (r = 0.74 & 0.75) and specifically with small granule cells (SGC). Cluster 7
313 markers (MOX and GPROT) specifically correlated (r = 0.68 and r = 0.56) with vesicular cells
314 (VC). Cluster 2 markers (EGFL and LEVAR) correlated positively with hyalinocytes (H) (r=0.85
315 and r=0.81). We could not identify specific markers for blasts and macrophage-like cells.

316

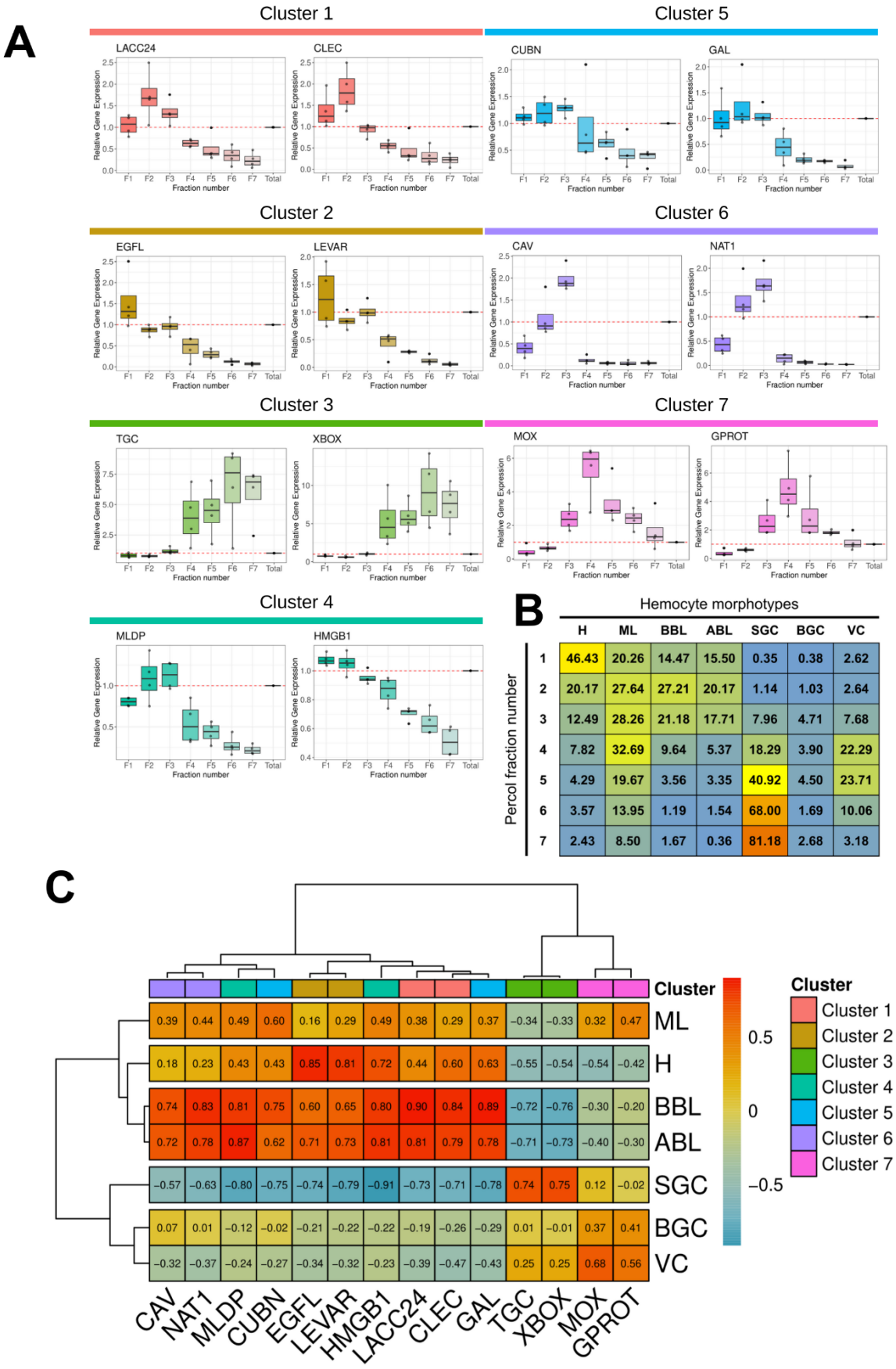
A
Cluster 1
LACC24
CLEC
Cluster 5
CUBN
GAL
Cluster 2
EGFL
LEVAR
Cluster 6
CAV
NAT1
Cluster 3
TGC
XBOX
Cluster 7
MOX
GPROT
Cluster 4
MLDP
HMGB1
Relative Gene Expression
Fraction number
F1 F2 F3 F4 F5 F6 F7 Total
B
Hemocyte morphotypes
Percol fraction number
H ML BBL ABL SGC BGC VC
1 46.43 20.26 14.47 15.50 0.35 0.38 2.62
2 20.17 27.64 27.21 20.17 1.14 1.03 2.64
3 12.49 28.26 21.18 17.71 7.96 4.71 7.68
4 7.82 32.69 9.64 5.37 18.29 3.90 22.29
5 4.29 19.67 3.56 3.35 40.92 4.50 23.71
6 3.57 13.95 1.19 1.54 68.00 1.69 10.06
7 2.43 8.50 1.67 0.36 81.18 2.68 3.18
C
Cluster
ML 0.39 0.44 0.49 0.60 0.16 0.29 0.49 0.38 0.29 0.37 −0.34 −0.33 0.32 0.47
H 0.18 0.23 0.43 0.43 0.85 0.81 0.72 0.44 0.60 0.63 −0.55 −0.54 −0.54 −0.42
BBL 0.74 0.83 0.81 0.75 0.60 0.65 0.80 0.90 0.84 0.89 −0.72 −0.76 −0.30 −0.20
ABL 0.72 0.78 0.87 0.62 0.71 0.73 0.81 0.81 0.79 0.78 −0.71 −0.73 −0.40 −0.30
SGC −0.57 −0.63 −0.80 −0.75 −0.74 −0.79 −0.91 −0.73 −0.71 −0.78 0.74 0.75 0.12 −0.02
BGC 0.07 0.01 −0.12 −0.02 −0.21 −0.22 −0.22 −0.19 −0.26 −0.29 0.01 −0.01 0.37 0.41
VC −0.32 −0.37 −0.24 −0.27 −0.34 −0.32 −0.23 −0.39 −0.47 −0.43 0.25 0.25 0.68 0.56
CAV NAT1 MLDP CUBN EGFL LEVAR HMGB1 LACC24 CLEC GAL TGC XBOX MOX GPROT
0.5
0
−0.5
Cluster
Cluster 1
Cluster 2
Cluster 3
Cluster 4
Cluster 5
Cluster 6
Cluster 7

317

318 **Fig 4. Characterization of the molecular markers specific to the different hemocyte**
319 **morphotypes. (A)** Relative expression level of the 14 markers in the different fractions after
320 gradient density sorting. The graphs show the relative expression of genes compared to their
321 expression in total hemocytes in the different fractions (red dotted line). Standard deviations were
322 calculated on four independent experiments. **(B)** Average percentage of each hemocyte type in the
323 7 Percoll gradient fractions used to quantify marker gene expression by qPCR. **(C)** Correlation
324 matrix between the relative gene expression of each marker gene in each fraction and the
325 percentage of each hemocyte type in the same fractions. Values and color scale represent the
326 Pearson correlation coefficient (r) ranging from -1 (inverse correlation) to +1 (full correlation).
327 **H** : Hyalinocyte, **ML** : Macrophage Like, **BBL** : Basophilic Blast Like cell, **ABL** : Acidophilic
328 Blast Like cell, **SGC** : Small Granule Cell, **BGC** : Big Granule Cell, **VC** : Vesicular Cell.
329 **LACC24** : Laccase 24, **CLEC** : C-type lectin domain-containing protein, **EGFL** : EGF-like
330 domain-containing protein 8, **LEVAR** : Putative regulator of levamisole receptor-1, **TGC** : TGc
331 domain-containing protein, **XBOX** : X-box binding protein-like protein, **MLDP** : ML domain
332 containing protein, **HMGB1** : High mobility group protein B1, **CUBN** : Cubilin, **GAL** : Galectin,
333 **CAV** : Caveolin, **NAT1** : Natterin-1, **MOX** : DBH-like monooxygenase protein 1, **GPROT** : G
334 protein receptor F1-2 domain-containing protein.

335

336 In conclusion, using RT-qPCR, cell sorting on Percoll gradients, and scRNA-seq analysis, we
337 were able to accurately identify cell types corresponding to three transcriptomic clusters. Cluster
338 3 corresponds to small granule cells (SGC), cluster 2 to hyalinocytes (H), and cluster 7 to
339 vesicular cells (VC). Cluster 3, cluster 2 and cluster 7 represent 17.8%, 23% and 3% of total cells
340 analyzed by scRNA-seq, respectively. This is consistent with cytology data in which we counted
341 12.5% +/- 5% Small Granule Cells, 30 +/- 9.3% Hyalinocytes and 2.3 +/- 1.6% Vesicular Cells
342 (**Fig. 1B and Fig. 3A**). Moreover molecular and cell functions deducted from GO-terms and

343 KEGG analyses (**Fig. 2**) were in agreement with the functions that could be expected to occur in
344 these three cell types.

345

346 **Only macrophage-like and small granule cells behave as professional phagocytes**

347 In order to gain further insights into hemocytes functional specialization, hemocytes separated on
348 the Percoll gradient were characterized functionally. Two hemocyte functions, namely
349 phagocytosis and production of Reactive Oxygen Species (ROS), are known to carry out major
350 cellular antimicrobial activities. Granular cells have been suggested to be the professional
351 phagocytes specialized for these functions (*30*). Here, phagocytosis and oxidative burst were
352 studied by using cell response toward zymosan particles (*31*).

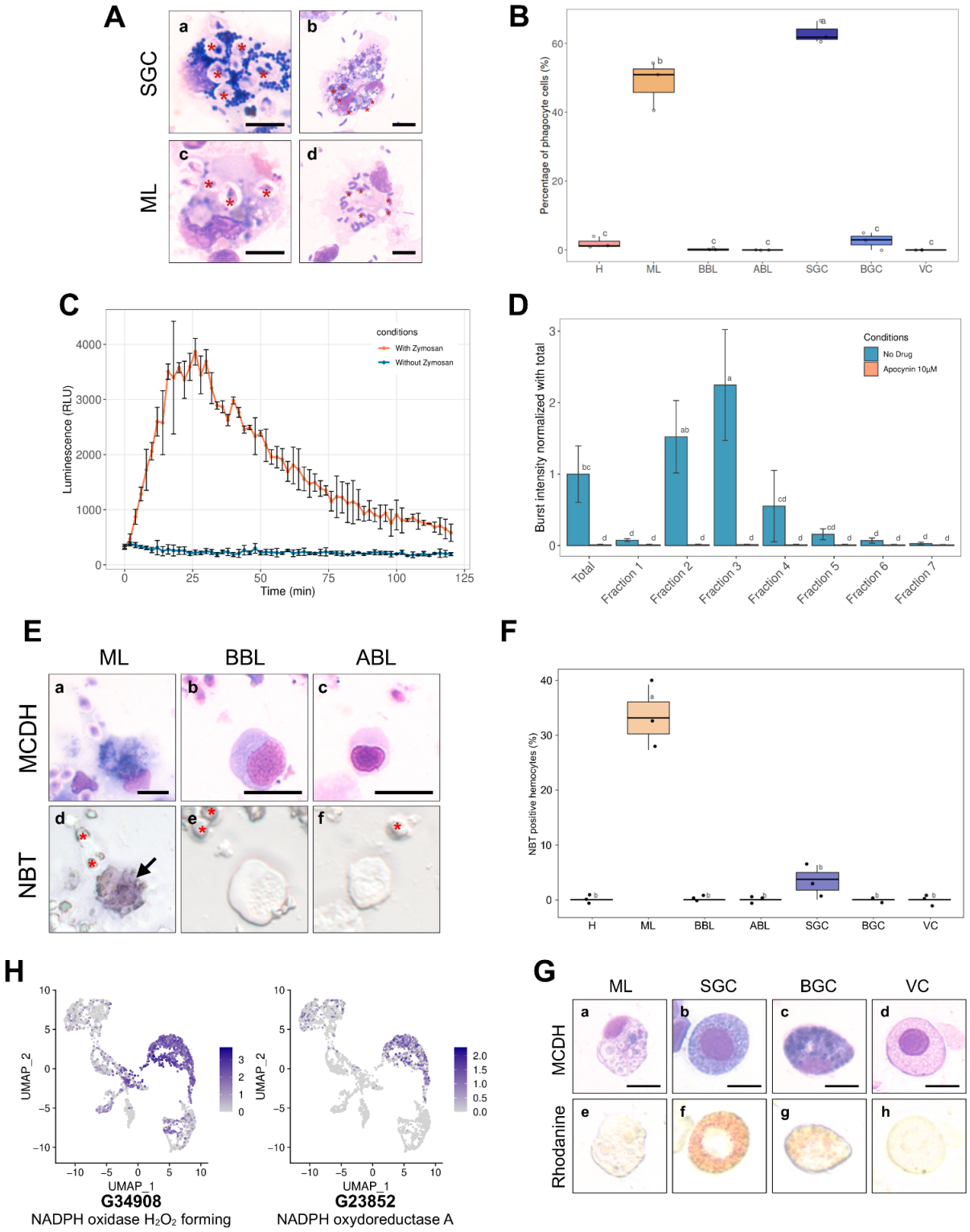

Fig 5. Phagocytosis, Reactive Oxygen Species production capacity and copper storage of hemocytes. (A) Images of small granule cells (**SGC**) and macrophage-like (**ML**) cells with phagocytosed zymosan particles (**panels a & c - red stars**) and *Vibrio tasmaniensis* LMG20012^{T} bacteria (**panels b & d - red stars**) from a total hemolymph sample. Scale bar : 5 µm. **(B)**

358 Quantification from 3 independent experiments of the phagocytic activity of each cell type for
359 zymosan particles. Results of the quantification of the phagocytic activity of each cell type. The
360 graph shows the result of 3 independent experiments. **(C)** Luminescence recording to detect the
361 production of Reactive Oxygen Species (ROS). In orange, biphasic curve obtained on naive
362 oyster hemolymph after zymosan addition at t = 0 min. In blue, the control condition corresponds
363 to hemocytes without zymosan addition. **(D)** Graph showing the intensity of ROS production in
364 each Percoll fraction. Normalized burst intensity was calculated from the luminescence peak
365 obtained from each fraction. In blue, no drug was added to the experiment, in orange, ROS
366 production was impaired by the addition of apocynin. **(E)** NBT (NitroBlueTetrazolium) staining
367 of hemocytes exposed to zymosan particles. Hemocytes morphology after MCDH staining :
368 Macrophage Like **(a)**, Basophilic **(b)** and Acidophilic **(c)** Blast cells. NBT staining of the
369 different hemocytes types **(d-f)**. Red stars show zymosan and bacteria particles. Black arrows
370 identify Macrophage-Like cells. Scale bar : 10 µm **(F)** Quantification of NBT-positive cells
371 present in the total hemolymph of oysters exposed to zymosan. **(H)** UMAP plots showing cells
372 expressing NADPH oxidase found in the scRNA-seq dataset and their expression level. **(G)**
373 Labeling of intracellular copper stores in *C.gigas* hemocytes. MCDH (upper panels) and
374 rhodanine (lower panels) staining of oyster hemocytes to reveal copper accumulation. Scale bar :
375 10µm. For panels **(B)**, **(D)** and **(F)** The alphabetic characters displayed above the data points in
376 each plot represent statistically significant differences among the groups, as determined by
377 Tukey's test following ANOVA. Groups denoted by different letters differ significantly from each
378 other at the $p < 0.05$ level of statistical significance. **H** : Hyalinocytes, **ABL** : Acidophilic Blast-
379 Like cells, **BBL** : Basophilic Blast-Like cells, **ML** : Macrophage-Like cells, **SGC** : Small Granule
380 Cells, **VC** : Vesicular Cells and **BGC** : Big Granule Cells.

381 The phagocytic activity of hemocytes was first tested on a sample of total oyster hemolymph.
382 Cells were incubated with either zymosan particles or the bacterial strain *Vibrio tasmaniensis*

383 LMG20012^T for 1 hour. Only the small granule cells and the macrophage-like possess an efficient
384 phagocytosis for both zymosan or vibrios, as observed after MCDH staining (**Fig. 5A, Supp. Fig.**
385 **6 and Supp. Fig. 7A**). Macrophage-like cells and small granule cells showed a phagocytosis
386 activity of 49% and 55% respectively, and a phagocytosis index of 3.5 and 5.2 particles per cell
387 respectively (**Fig. 5B and Supp. Fig. 7B**), as confirmed in 3 independent experiments. Very
388 limited phagocytic activity was observed for hyalinocytes (1.7%), basophilic blasts (0.18%), and
389 big granule cells (2.7%) with a phagocytosis index of 2, 1, and 2.5 particles per cell, respectively
390 (**Fig. 5B and Supp. Fig. 7B**). These results confirmed that only small granule cells and
391 macrophage-like cells behave as professional phagocytes harboring a strong phagocytosis
392 activity.

393

394 **Only macrophage-like cells produce Reactive Oxygen Species**

395 We next examined the ability of *C. gigas* hemocytes in each Pecoll fraction to produce Reactive
396 Oxygen Species (ROS) upon stimulation by zymosan using the Luminol oxidation assay. Luminol
397 luminescence peaked 25 minutes after hemocyte (isolated from total hemolymph) were exposed
398 to zymosan, which corresponds to a robust oxidative burst (**Fig. 5C**). The ROS production was
399 dependent on a NADPH oxidase, as it was completely inhibited by the NADPH oxidase specific
400 inhibitor apocynin (**Fig. 5C**). To identify which hemocyte types were involved in ROS production
401 we tested Percoll density sorted hemocytes for oxidative burst activity. Fractions 2 and 3
402 displayed higher oxidative burst activity than the other fractions. The burst intensity of fraction 3
403 was twice that of total hemocytes, and fraction 2 also exhibited significantly increased burst
404 activity. In contrast, fraction 4, showed a significant decrease in oxidative burst, and no activity
405 was observed for fractions 1, 6 and 7 (**Fig. 5D**). These results indicate that NADPH-dependent
406 oxidative burst activity is carried out by fractions enriched in macrophage-like (ML) cells and
407 blast-like cells (ABL and BBL).

408 Previous studies have demonstrated that granular cells produce ROS (*30*). In contrast, we found
409 that small granule cells collected in fraction 7 were incapable of producing ROS through an
410 oxidative burst. To identify which type of hemocyte from blast-like cells and macrophage-like
411 cells produce ROS within a few minutes after exposure to zymosan, ROS production was
412 investigated using NitroBlueTetrazolium (NBT) reduction to directly stain hemocytes. This
413 allows correlative microscopy using MCDH staining after the NBT reduction reaction.
414 Macrophage-like cells were strongly and significantly stained by NBT reduction (33.2%) (**Fig.**
415 **5E, panels a & d**) while some small granule cells were lightly stained by NBT reduction (**Fig.**
416 **5F**). Blast-like cells, big granule cells, vesicular cells, and hyalinocytes were never NBT stained,
417 confirming that these cell types were not involved in ROS production (**Supp. Fig. S7**).
418 Altogether, these observations showed that small granule cells and macrophage-like cells are the
419 two professional phagocytes among hemocytes but only macrophage-like cells are capable of
420 oxidative burst upon exposure to zymosan. Based on these new functional data we further
421 analyzed the expression level of NADPH-oxidase related enzymes in the scRNA-seq dataset.
422 Cells of the cluster 1 were found to predominantly express two NADPH oxidase isoforms (gene
423 numbers G34908 and G23852) compared to other clusters (**Fig. 5H**). Additionally, this cluster
424 expresses macrophage-specific genes such as the angiopoietin receptor (**Table 1**), as well as
425 maturation factors for dual oxidase, an enzyme involved in peroxide formation (**Supp. Fig. S8**).
426 Collectively, these data indicated that cells of the transcriptomic cluster 1 corresponded to
427 macrophage-like cells.

428

429 **Small granule cells and big granule cells accumulate intracellular copper**

430 The effect of copper on oyster hemocytes has long been studied due to its abundance in polluted
431 marine areas (*21*). In addition, several studies have shown that *Vibrio* species pathogenic for *C.*
432 *gigas* possess copper resistance genes, which are essential to survive inside hemocytes (*32*).

433 Therefore, we investigated which hemocyte types are involved in copper metabolism. To this end,
434 total hemocytes isolated from naive oysters were stained with rhodanine to reveal copper storage
435 in cells. Rhodanine staining revealed that 33 +/- 2 % of small granule cells and 30 +/- 10 % of big
436 granule cells exhibited a specific reddish/brown staining indicative of high concentration of
437 copper in their granules specifically (**Fig. 5G and Supp. Fig. S9**). These results provide the
438 functional proof that SGC are specialized in metal homeostasis in addition to phagocytosis, as
439 suggested by the scRNAseq data (Cluster 3).

440 **Antimicrobial peptides are expressed by agranular cells, blasts and hyalinocytes**

441 Antimicrobial peptides (AMPs) have long been studied for their role in invertebrate humoral
442 immune response, and have been shown to be expressed by hemocytes including in *C. gigas* (*33*).
443 We investigated whether different AMPs were expressed by different hemocyte cell types.
444 Unfortunately, scRNA-seq analysis was not sensitive enough to reveal AMPs expression due to
445 the limited sequencing depth, so we investigated AMPs expression by RT-qPCR on Percoll
446 density fractionated hemocytes. Cg-Bigdefs 1-2, Cg-BPI and hemocyte defensin were found to be
447 expressed mostly by agranular cells, blasts and hyalinocytes (ABL, BBL and H) (**Fig. 6A, B and**
448 **C**). Among them, the expression of the four AMPs correlated with Blasts abundance whereas the
449 expression of Cg-BigDefs 1-2 only correlated with hyalinocytes s (**Fig. 6D**). Granular cells (VC,
450 ML, BGC and SGC) did not seem to express any of the AMPs that were analyzed here. These
451 data suggest that some of the agranular cells are specialized in the production of humoral
452 effectors.

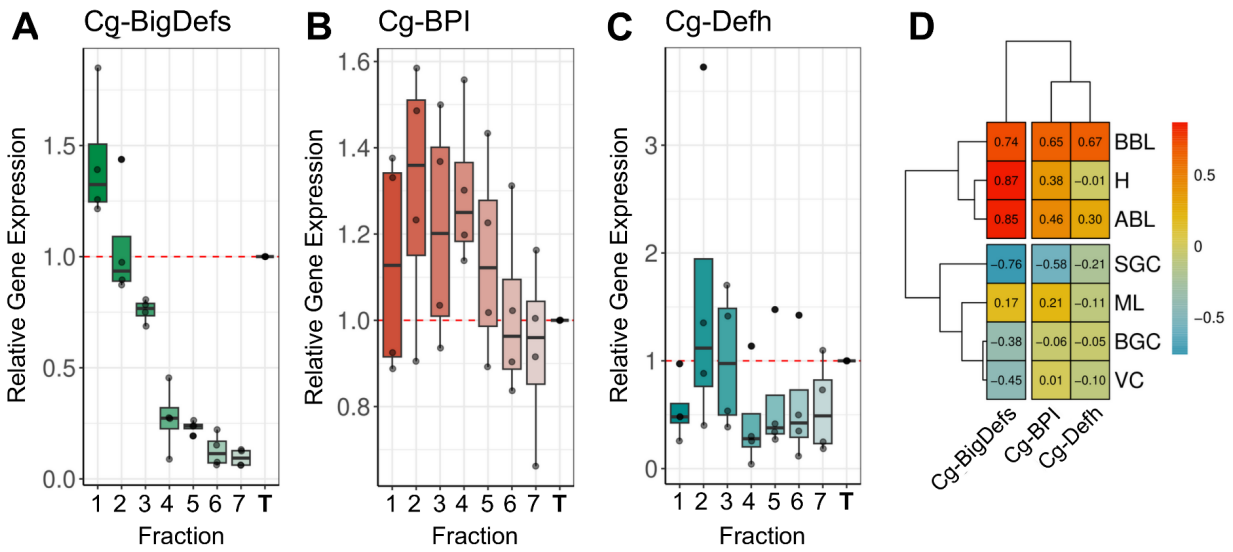

Fig 6. Hemocyte expression profiles of some antimicrobial peptides. (A) (B) and **(C)** Relative Gene Expression in the 7 Percoll hemocyte fractions of Big-Defensin1 & 2 (Cg-BigDefs), BPI (Cg-BPI) and hemocyte defensin (Cg-Defh) respectively compared to the gene expression level in unfractionated hemolymph. **(D)** Correlation matrix between the relative gene expression of BigDefensin1 & 2, BPI and hemocyte defensin gene in each fraction and the percentage of each hemocyte type in each fraction (**H** : Hyalinocytes, **ABL** : Acidophilic Blast Like, **BBL** : Basophilic Blast Like, **SGC** : Small Granule Cell, **ML** : Macrophage Like, **BGC** : Big Granule Cell, **VC** : Vesicular Cell. Values and color scale represent the Pearson correlation coefficient (r) ranging from -1 (inverse correlation) to +1 (full correlation).

Tentative model of hemocyte lineages and differentiation pathways in *C. gigas.*

Ontogeny, lineage and differentiation pathways are still mostly unknown in bivalves (*34*), but there are some clues for the presence of circulating and proliferating hemocytes progenitors in the hemolymph of *C. gigas* (*35*). GO-terms analysis of the 7 transcriptomic clusters revealed different functional signatures, among them the transcriptomic signature of the cluster 4 revealed a high expression level of ribosomal proteins (**Supp. Fig. S1J**), a particularity found in hematopoietic

stem cells in vertebrates (*36*) (*37*) (*38*). In addition, thanks to scRNAseq approaches, it is now possible to deduce differentiation pathways from mRNA splicing variant analysis using bioinformatic tools like Monocle3 (*39*). This revealed the overexpression of genes involved in the splicing, transcription and translation continuum in the same fourth cluster (**Fig. 2**) reinforcing the hypothesis of a pool of quiescent or immature cells capable of engaging in differentiation upon stimulation.

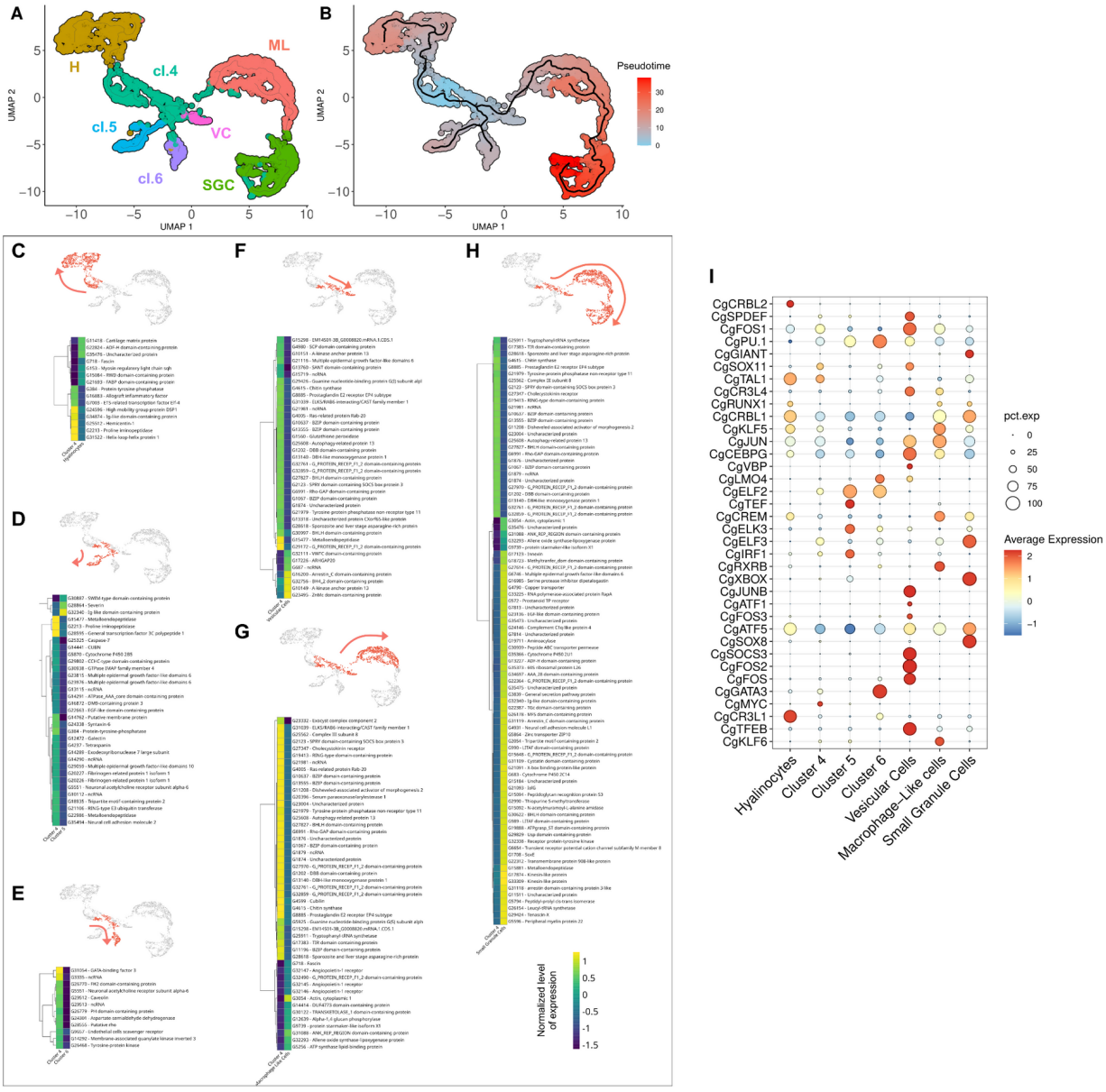

Figure 7. Pseudotime ordering of cells revealed 6 potential differentiation pathways of hemocytes. (A) UMAP plot of scRNA-seq analysis showing the 7 transcriptomic clusters used

479 for pseudotime analysis. 4 clusters were identified cytologically (SGC for small granule cells -
480 cluster 3, H for hyalinocytes - cluster 2, ML for Macrophage Like - cluster 1 and VC for vesicular
481 cells - cluster 7), cl.4, cl.5, and cl.6 represent clusters 4, 5, and 6, respectively. **(B)** Graphical
482 representation (UMAP projection) of the Monocle 3 pseudo-time order of the clustered cells.
483 Cluster 4 (cl.4) was used as the origin for the pseudotime analysis. **(C) (D) (E) (F) (G) and (H)**
484 show gene expression level of selected marker genes obtained from the monocle3 trajectory
485 analysis at the beginning and end of the modelized differentiation pathways (in red on the UMAP
486 plot) from cluster 4 to hyalinocytes, to cluster 5 cells, to cluster 6 cells, to Vesicular Cells (VC),
487 to Macrophage-Like cells (ML) and to Small Granule Cells (SGC) respectively. The color scale
488 represents the normalized expression level of each gene. **(I)** Dot plot showing the average
489 expression and the percentage of cells expressing identified transcripts encoding for transcription
490 factors in the scRNA-seq dataset. Average expression is expressed in Log2FC.

491

492 Therefore, cluster 4 was chosen to enroot the pseudotime analysis to deduce differentiation
493 pathways and cell lineages using Monocle3. (**Fig. 7A**). By temporally ordering the 2817 cells
494 analyzed by scRNA-seq 5 cell lineages could be defined (**Fig. 7B**). Differentiation pathway 1
495 leads to hyalinocytes (H) (**Fig. 7C**). This transition is characterized by the downregulation of 8
496 genes, two of which are transcription factors (G7003 and G31522). The hyalinocyte cluster was
497 also characterized by the overexpression of genes involved in cell contractility (G22824, G153
498 and G11418). Differentiation pathway 2 leads to cells of cluster 5 and are characterized by the
499 downregulation of about 30 genes, and 3 genes related to Zn finger protein, actin cleavage and Ig-
500 like domain proteins were specifically overexpressed (G30887, G28864 and G32340) (**Fig. 7D**).
501 Differentiation pathway 3 leads to cells of cluster 6 and is characterized by the down-expression
502 of 12 genes, and the upregulation of a GATA family transcription factor (G31054) (**Fig. 7E**).
503 Pathways between cluster 4, 5 and 6 found by Monocle3 analysis were pseudo temporally short

504 and few specific markers were identified, suggesting that they were transcriptionally close.
505 Differentiation pathway 4 leads to vesicular cells (VC) (**Fig. 7F**) where a large number of genes
506 were silenced to give rise to these cells. Seven genes were specifically overexpressed in the VC
507 (G32111, G17226, G687, G16200, G32756, G10149 and G23495). Interestingly, 6 genes
508 encoding potential transcription factors were downregulated in this lineage (G30997, G10637,
509 G1067, G13555, G2123 and G27827). Differentiation pathway 5 leads to macrophage-like cells
510 (ML), and is characterized by the underexpression of 35 genes and the overexpression of 13
511 genes. Among the 35 genes, 6 of them were putative transcription factors (G2123, G10637,
512 G13555, G27827, G1067 and G11196) (**Fig. 7G**). Finally, we can delineate a lineage ending in
513 small granule cells (SGC) (**Fig. 7H**). This pathway involved cluster 4 (immature cells), VC, ML
514 and SGC and was characterized by the downregulation of 27 genes, including 5 potential
515 transcription factors (G10637, G13555, G27827, G1067 and G2123). SGC showed a distinct
516 transcriptomic signature with 61 overexpressed genes, including 3 transcription factors (G1708,
517 G21091 and G30622). Taken together, we propose that immature cluster 4 cells have pluripotent
518 potential and can give rise to four terminally differentiated cell types which are cluster 5 and 6
519 cells, hyalinocytes and small granule cells and two other transient hemocyte cell types : vesicular
520 cells and macrophage-like. All data from the Monocle3 analyses are available as Supplementary
521 Data (**Supp. Fig. S10**).

522 Differentiation pathway analysis thus revealed the over- or under-expression of various
523 transcription factors in the identified pathways. As transcription factors are well known master
524 regulators of cell differentiation and can help to delineate cell lineages, we investigated
525 combinatorial expression patterns of transcription factors among the different transcriptomic cell
526 clusters. Based on GO-terms annotation we could isolate 28 different sequences corresponding to
527 transcription factors from the scRNA-seq dataset. The transcription factor function was confirmed
528 by manual annotation (**Supp. Table S5**) and **Figure 7I** shows the average expression profiles of

529 them in the different clusters and **Supplementary Figure S11** their expression levels in single
530 cells. Two transcription factors, CgATF5 and CgCRBL1 displayed a contrasting expression
531 profile with an increased average expression in macrophage-like cells, hyalinocytes and small
532 granule cells versus a low expression profile in cells in clusters 4, 5, 6 and vesicular cells. We also
533 identified transcription factors that were specifically expressed in the different transcriptomic
534 clusters : CgSPDEF, CgSOCS3, CgFOS and CgTFEB were specific for vesicular cells, CgSOX8,
535 CgXBOX and CgELF3 were specific for small granule cells, CgCR3L1 and CgTAL1 for
536 hyalinocytes, and CgJUN, CgKLF5, CgKLF6 and CgCREM for macrophage-like cells. Eight
537 other transcription factors were specifically identified in cluster 6 (CgGATA3, CgPU.1 and
538 CgELF2), cluster 5 (CgELF2, CgELK3 and CgIRF1) and cluster 4 (CgTAL1 and CgFOS1).
539 These data define potentially four distinct hematopoietic lineages originating from one type of
540 immature blast cells and give rise to hyalinocyte, SGC (via VC and ML), or two distinct
541 differentiated blast-like cells. We also identified a combination of transcription factors specific to
542 lineages and cell types that are potential master regulators of cell fate during hematopoiesis.

543 **Discussion**

544 The results of our study significantly improve the knowledge of *C. gigas* hemocyte functional
545 diversity and lineages. Using a combination of Single-cell RNA-seq and cytology, we identified
546 seven distinct hemocyte transcriptomic cell clusters, and the same number of morphotypes: four
547 granular cell types (big granule cells, macrophage-like cells, small granule cells and vesicular
548 cells), two distinct blast-like cells (basophilic and acidophilic blast-like cells), and one agranular
549 epithelial-like cell type (hyalinocytes). A major challenge was to find correlations between
550 transcriptomic and cytological data in order to fully define each distinct cytological cell type. This
551 challenge was overcome by combining multiple approaches using isopycnic Percoll density
552 gradient fractionation combined with expression of transcriptomic markers and functional assays
553 including phagocytosis, oxidative burst, copper accumulation, AMP expression and finally

554 pseudotime analysis of gene expression. All these results confirmed the historical classification of
555 the 3 main cell groups : blasts, hyalinocytes and granular cells (*15*) and provided deeper insight
556 into functional specificities of poorly characterized cell types. Particularly, we highlighted
557 distinct transcriptional and functional subtypes among blasts and granular cells with
558 complementary immune specialization and lineage relationships between cells.
559
560 One major result of the present study is the identification of cell types performing antimicrobial
561 functions such as phagocytosis, accumulation of intracellular copper, an oxidative burst and
562 antimicrobial peptide production, which have been extensively studied for their role in
563 antibacterial and antiparasitic defenses as they are found in the large majority of invertebrates
564 (*17*). However, the cell types specialized for these critical immune functions in bivalves, and in
565 particular in oysters, have long been debated and the involvement of the different hemocyte
566 subpopulations in immune functions has remained poorly understood.
567
568 Here, we uncover that the macrophage-like (ML) and the small granule cells (SGC) are the only
569 hemocyte cell types that behave as professional phagocytes, as evidenced against Zymosan or
570 *Vibrio*. These two distinct cell types could be distinguished functionally. First, we identified two
571 distinct transcriptomic clusters for each cell type (Cluster 1 for ML / BGC and Cluster 3 for
572 SGC). Second, only ML performed a measurable oxidative burst. Third, only SGC accumulated
573 intracellular copper in specific granules. The two types of professional phagocytes belong to the
574 same granular cell lineage, as determined by pseudotime analysis. The fact that ML could serve as
575 a precursor for SGC could be counterintuitive. However, this is not an isolated case in
576 invertebrate hemocytes. For instance, in *Drosophila* larvae (*40*), some populations of professional
577 phagocytes, the sessile plasmatocytes, give rise to crystal cells or lamellocytes that are
578 morphologically and functionally distinct from plasmatocytes (*41*). Like in the oyster, the

579 existence of multiple professional phagocytes is reminiscent of vertebrates macrophages,
580 polynuclear neutrophils and dendritic cells, which harbor distinct functional specialization like
581 efferocytosis (*42*), oxidative burst, NETosis, or antigen presentation (*43*).
582
583 The characterisation of professional phagocytes in oysters is of particular importance to better
584 understand oyster-*Vibrio* interactions during pathogenesis. Some of the best studied oyster
585 pathogens, including strains of *V. tasmaniensis* or *V. aestuarianus francensis* harbor virulence
586 traits that allow them to interfere with phagocytic activity of hemocytes during pathogenesis as,
587 for example, *V. tasmaniensis* that behaves as a facultative intracellular pathogen with
588 phagocytosis-dependent cytotoxicity (*44*). Both *V. tasmaniensis* and *V. aestuarianus* also harbor
589 resistance to copper toxicity through CopA and CusA/B transporters; this trait is essential for the
590 survival and virulence in oyster (*45*), *32*). As we characterized here that SGCs are professional
591 phagocytes with copper-rich granules, it is likely that the cellular interactions between SGCs and
592 these vibrios is critical during antibacterial host response and pathogenesis. ML are phagocytes
593 that harbor a very potent NADPH-oxidase dependent oxidative burst. Oxidative burst is
594 recognized as a very rapid and potent antimicrobial response for professional phagocytes like
595 Polynuclear neutrophils in mammals. Interestingly, NADPH dependent ETosis has been reported
596 in *C. gigas i*n a similar manner than human neutrophils (*46*), this cell death is characterized by the
597 projection of DNA extracellular traps that capture and kill some pathogens like *Vibrio* (*47*).
598 Hence, it is tempting to speculate that ML could be also involved in ETosis.
599
600 The specialized functions harbored by the two other types of granular cells, the BGCs and the
601 VCs, remain more elusive. A specific scRNAseq transcriptomic cluster for BGCs was difficult to
602 identify, still, the level of expression of laccase 24 was found higher in a particular subcluster
603 among ML (**Supp. Fig. S8**) and pseudo-time analysis highlighted the same subcluster as an

604 alternative differentiation state among ML (**Fig. 7B**). The enrichment of transcripts involved in
605 oxido-reduction pathways, laccase 24 in particular, is in accordance with their potential role in
606 melanisation and response to oxidative stress (*48*). Although melanin-like deposits have been
607 observed in some cases of infestation by the parasites *Martelia* or B*onamia* in the Sydney rock
608 oyster (*49*), this mechanism is not as strong as what is described in arthropods, which perform
609 melanization through a prophenoloxidase activation cascade (*50*), (*51*). In many marine
610 invertebrates (*48*), one type of hemocytes known as Brown Cells could relate to the BGCs that we
611 describe here. In fact, when observed without any staining (as in **Fig. 5F**), their big granules with
612 a yellow to dark brown content appears to correspond well with the historical description of
613 brown cells that often infiltrate tissues (like gills) in animals exposed to polluted waters (*48*).
614 These cells have thus been thought to be involved in detoxification processes. Based on our
615 pseudotime analysis, we show that they likely derive from ML but with limited phagocytosis
616 activity and rather specialized in melanisation and potentially heavy metal detoxification, as
617 evidenced by rhodanine staining showing copper accumulation in some of their granules (**Fig.**
618 **5G**). To better understand the role of BGCs further studies should be performed either upon
619 parasitic infestation or exposure to toxic stresses.
620 Finally, VC are granular cells that remain to be functionally characterized. They possess a strong
621 intracellular vesicular trafficking and autophagy activity, as deduced from their transcriptomic
622 profile. Still, we could not identify a particular immune-related function based on our functional
623 assays. Their clear granules appear auto-fluorescent when illuminated with UV light (**Supp. Fig.**
624 **S11**) but the biochemical nature of the content of these granules remains to be characterized. As
625 they also appear as cell intermediate along the granular cell differentiation pathway in pseudotime
626 analysis, they could represent functionally immature precursors of the other three granular cell
627 types, like promyelocytes that possess specific azurophilic granules but are functionally immature
628 precursors during granulocytes differentiation in human. However the enrichment of autophagy

629 related transcripts in VC calls for further investigation of a potential role in antiviral immunity as
630 autophagy has been suggested to play a role in the response to OsHV-1 virus (*52*).
631
632 Hyalinocytes represent an homogenous cell type with only one morphotype matching one
633 transcriptomic cluster. They originate from a specific and very different differentiation pathway
634 than the granular cells, as deduced from pseudotime analysis. According to the literature,
635 hyalinocytes are involved in the early stages of inflammation and can infiltrate wounds and
636 interact with foreign particles. In the flat oyster *Ostrea edulis*, they contribute to shell production
637 and wound healing (*53*). In the Sydney rock oyster they play a role in cell n aggregation (*54*),
638 while in *C. virginica* (*55*) they contribute to encapsulation, which is reminiscent of lamellocytes
639 in *Drosophila*. Our results indicate an important role in the immune response is their expression
640 of antimicrobial peptides (AMPs). Indeed, *Cg*-BigDefs, which participates in the control of oyster
641 microbiota (*56*), were found to be expressed both in hyalinocytes and blast-like cells. Supporting
642 this immune function, hyalinocytes from the oyster *O. edulis* have been shown to express the
643 AMP Myticin C (*57*). Among AMPs, we also identified that Cg-BPI and *Cg*-Defh, are more
644 expressed in BBL, ABL than in other cell types. These results are somewhat unexpected as AMPs
645 have often been considered to be stored in granules of granular cells but not in agranular cells
646 (*16*). These results urge the need to reconsider a particular role for some agranular cell types in
647 the active production of humoral immune effectors. Based on our findings, it can be hypothesized
648 that hyalinocytes and/or the blast-like cells are a cellular target of the OsHV-1 virus, the causal
649 agent of POMS, which dampens the expression of certain AMPs (*58*), thereby inducing a
650 bacterial dysbiosis. Whether this is due to a decreased expression of AMPs and/or an inhibition of
651 immature blast cells differentiation involved in the renewal of agranular cell types remains to be
652 established.
653

One limit of our study is that we could not decipher the full complexity of blast-like cells, as we identified 3 clusters and only 2 morphotypes. Cell fractionation using Percoll gradient could not yield pure blast-enriched fractions (ABL and BBL), making precise functional characterization impossible. The enrichment in transcripts of the transcription synthesis degradation continuum aligns with the definition of undifferentiated blast-type cells and with the basophilic staining obtained in MCDH for BBL cells as immature blast cells are characterized by a basophilic cytoplasmic staining in human. However, our results show that some of these blast populations have the ability to produce AMPs, suggesting that these cells can also actively participate in the production of humoral effectors. Finally, whether these circulating immature cells are truly the stem cells at the origin of all hemocytes remains an open question.

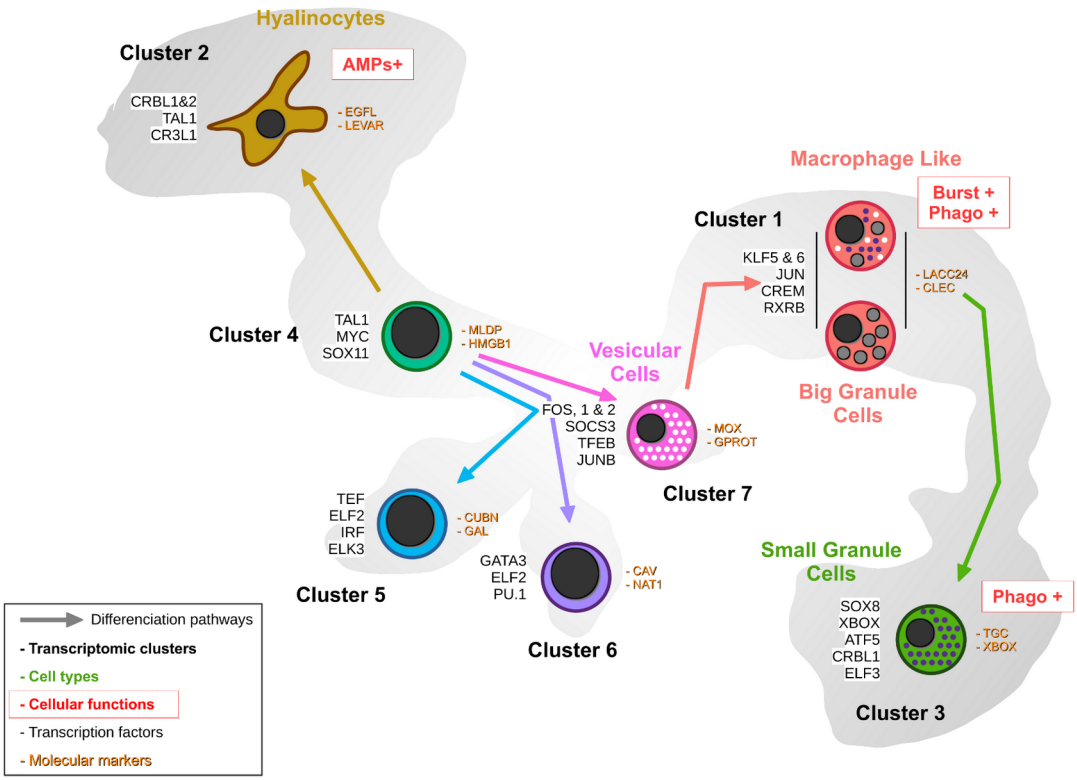

Figure 8. Proposed hemocyte ontology in *Crassostrea gigas* based on the transcriptomic, cytological and functional results obtained. Cells are shown colored according to the same

color code as the transcriptomic clusters. Cluster numbers and cell types are indicated. To the left of the cells are noted the overexpressed transcription factors and to the right the identified marker genes in each cluster. Functional characteristics of hyalinocytes, macrophage-like and small granule cells are marked in red.

In the animal kingdom, the innate immune system relies on specialized cells derived from pluripotent precursors through hematopoiesis. Transcription factors in particular have been found to be well conserved throughout the life kingdom from invertebrates to vertebrates. However in bivalves, the mechanisms underlying their functional differentiation are only partially available or understood (*59*). Recent researches have suggested the existence of potential hemocyte progenitors, also known as blast-like cells in several bivalve species, including clams, mussels, scallops, marine mussels, freshwater mussels, oysters, pearl oysters, and wing shells (*59*), however different models for hematopoiesis in bivalve have been proposed and long been debated without a clear consensus and definitive proofs. Thanks to single-cell RNA sequencing and pseudotime analysis, we can now propose a refined model of hematopoiesis at an unprecedented level of detail. In this model, the different types of hemocytes are likely produced through four differentiation pathways originating from a common progenitor. One pathway leads to the formation of agranular hyalinocytes, while another independent pathway gives rise to the granular cells, including VC, ML, BGC, and SGC. Additionally, there are two other differentiation pathways that potentially lead to terminally differentiated blast-like cells. The differentiation of mature hemocytes involves the establishment of lineage-specific gene expression profiles that rely on transcription factors to modulate the expression of their target genes. Here, we identified combination of transcription factor that are differentially expressed during *C. gigas* hematopoiesis and are specific of differentiation stages and cell lineages, among them many well-known

692 hematopoietic transcription factors like GATA, PU-1, TAL1 and SOX factors are positioned in
693 this model of *C. gigas* hematopoiesis (*60*), (*61*), (*62*) (**Fig. 8**).
694 Our study significantly advances our understanding of bivalve immunity, particularly in
695 comparison to arthropods. By introducing a standardized reference hemocytogram for oysters
696 using MCDH staining, defining cell type specific markers, and key transcription factors likely
697 involved in cell fate determination, and clarifying the functions of different hemocytes, we set the
698 ground for future in depth studies. This will allow further studies of the oyster's immune response
699 to various biotic and abiotic stress at the cellular level. A better comprehension of antiviral and
700 antibacterial responses in bivalves and improving our understanding of immune priming and
701 immune memory at the cellular level in bivalves will improve health and population management
702 for sustainable aquaculture production. Moreover, they will contribute to the broader field of
703 evolutionary immunology by enabling comparative studies and deciphering the diversification of
704 immune cells and immunity related genes in a protostome.
705

706 **Materials and Methods**

707 **Conservation of oysters**

708 The work described here was performed using two different sources of oysters of the same
709 species *Crassostrea (Magallana) gigas*. ISA (Ifremer Standardized Oysters - La tremblade -
710 France) oysters for the scRNA-seq experiment and oysters provided by a local supplier
711 (https://www.huitres-bouzigues.com). Animals were washed and kept in 10 L tanks containing
712 seawater and a bubbler to oxygenate and homogenize the water. Water was changed daily and
713 oyster health was monitored. All animals used in this study were 18 months of age.

714 **Hemocyte collection and processing**

715 *Crassostrea gigas* hemocytes were obtained by puncture of the adductor muscle from live
716 animals. The oyster shell was incised with forceps on the posterior side. Hemolymph was

717 collected using a 23Gx1" needle mounted on a 5 mL syringe prefilled with 2 mL of ice-cold
718 Alsever modified medium (20.8 g glucose – 8 g trisodium citrate - 22.5 g sodium chloride - 0.4 g
719 BSA - pH=7.5). Samples were centrifuged for 4 minutes at 200 g – 4 °C and the supernatant was
720 removed and replaced with 1 mL of fresh Alsever modified medium. Each hemocyte sample was
721 thoroughly checked for quality, counted under a microscope using KOVA (Kova International,
722 USA) slides, and stored on ice prior to processing. For scRNA-seq analysis, resuspended
723 hemocytes were filtered on 30 µm filters, counted, the solution was adjusted to 1.10^6 cells per mL
724 and stored on ice prior to 10X genomic library preparation.

725 ***C. gigas* genome annotation**

726 The *C. gigas* genome (Genbank GCA_905397895.1) (*27*) was used as a reference. Prior to
727 annotation, the longest CDS sequences were extracted from the gff3 file. Annotation was realized
728 using the ORSON script (https://gitlab.ifremer.fr/bioinfo/workflows/orson). ORSON combines
729 state-of-the-art tools for annotation processes within a Nextflow pipeline. ORSON script performs
730 sequence similarity search with BLAST (*63*) against Uniprot-Swissprot and Uniprot-trEMBL
731 database, and functional prediction with InterProScan (*64*) and eggNOG (*65*) orthogroup
732 annotation. Interproscan analysis was performed against Pfam, Prosite, CDD, TIGR, SMART,
733 SuperFamily, PRINTS and Hamap databases. Results were collected and processed using
734 Blast2GO (*66*) for annotation mapping and validation.

735 **Drop Seq based scRNA-seq library generation**

736 The 10X Genomics protocol, Single Cell 3' Reagent Kits v2 User Guide from the manufacturer
737 (10X Genomics, USA) was followed to prepare gel in emulsion beads (GEM) containing single
738 cells, hydrogel beads, and reverse transcription reagents, perform barcoded cDNA synthesis, and
739 generate sequencing libraries from pooled cDNAs. The concentration of single cell suspensions
740 was approximately 1000 cells / µL, as estimated by manual counting, and cells were loaded
741 according to the 10X protocol to capture approximately 3000 cells per reaction. Library

742 construction (after GEM digestion) was performed using 10X reagents according to the
743 manufacturer. Libraries (paired end reads 75 bp) were sequenced on an Illumina NovaSeq
744 (Illumina, USA) using two sequencing lanes per sample.

745 **scRNA-seq analysis**

746 Reads were aligned to the *C. gigas* reference genome (Genbank GCA_905397895.1) (*27*) using
747 STAR solo software (v 2.7.10) (*23*). Unique molecular identifiers (UMIs) were extracted and
748 counted for each cell, and an expression matrix was generated for further analysis. Single-cell
749 RNA sequencing (scRNA-seq) data analysis was performed using the R programming language
750 (version 4.2.1) (R Core Team, 2018) and the Seurat package (version 4.3.0) (*67*). The data were
751 then pre-processed to remove unwanted sources of variation and to normalize gene expression.
752 Cells with small library sizes and a high proportion of mitochondrial genes were excluded. Data
753 normalization was performed using the SCTransform method. After normalization, highly
754 variable genes were identified using the FindVariableFeatures function and the top variable genes
755 were selected for downstream analyses. Dimensionality reduction was performed using Principal
756 Component Analysis (PCA), subsequently, uniform manifold approximation and projection
757 (UMAP) was applied to visualize the data. Cell clustering was performed using the 'FindClusters'
758 function, using the previously identified significant principal components (dims = 6) and a
759 resolution parameter (r = 0.1) to define cluster granularity. Differential expression analysis was
760 performed using the 'FindAllMarkers' (pct.min = 0.25) function to identify genes differentially
761 expressed between clusters, with statistical significance determined using the Wilcoxon rank sum
762 test. Functional enrichment analysis of differentially expressed genes was performed using gene
763 set enrichment analysis (RBGOA) (*68*).

764 **KEGG pathway analysis**

765 KEGG analysis was performed using DAVID Bioinformatics Resources (NIAID/NIH) (*26*). Gene
766 lists of specifically overexpressed genes in each cluster were obtained after scRNA-seq

767 processing (genes with Log2FC > 0.25 and significant p-value < 0.001) and used for KEGG
768 annotation. The *C. gigas* reference genome from the DAVID bioinformatics resource was used
769 for this analysis, with thresholds of 2 for counts and 0.05 for EASE value (p-value). KEGG
770 annotation results were post-processed and presented as a heatmap showing KEGG pathway, fold
771 enrichment, p-value significance and number of positive terms.

772 **Rank Based Gene Ontology Analysis**

773 RBGOA first clusters GOs according to their representative genes to identify the most significant
774 GOs, and then ranks the identified biological processes according to their average expression
775 levels (over all representative genes). Finally, biological processes, molecular functions and
776 cellular components significantly enriched in DEGs are identified by a Mann-Whitney rank test
777 with a strict FDR correction. The files generated by the GO-MWU scripts
778 (https://github.com/z0on/GO_MWU) were post-processed to extract the category names and the
779 fraction indicating the number of "good candidates" relative to the total number of genes
780 belonging to that category. The "good candidates" were the genes that exceed an arbitrary
781 'absValue' cutoff (defined as 0.001) in their significance measure. The results were presented as a
782 heatmap.

783 **Percoll Density Gradient Separation of Hemocytes**

784 A concentration series of Percoll (Cytiva, Sweden) diluted in Alsever modified medium was
785 prepared as follows: 10, 20, 30, 40, 50, 60 and 70 % (vol/vol). Discontinuous density gradients
786 (from 10 % Percoll with a density of 1.0647 to 70 % Percoll with d=1.1049) were made using 1.5
787 mL of each concentration and loaded with 1 mL of the hemocyte suspension corresponding to
788 approximately 2.10^7 cells. Centrifugation was performed (30 min, 800 g, 4 °C) in a swinging
789 bucket on a Beckman Coulter JS-13.1 rotor (Beckman Coulter, USA). Hemocytes concentrated at
790 each density interface were collected separately with a 70 mm long 20Gx2.75" needle mounted
791 on a 1 mL syringe. The hemocytes were then washed from the Percoll by adding 10 mL of ice-

792 cold Alsever modified medium, pelleted by centrifugation (10 min, 200 g, 4°C) and resuspended
793 in Alsever modified medium or filtered sea water.

794 **Cytological description of the hemocyte populations**

795 200,000 fresh hemocytes were seeded onto a slide using a Cytospin 4 centrifuge (Thermo
796 Scientific, USA). The samples were then stained using the panoptic MCDH (Micro Chromatic
797 Detection for Hematology) (Cellavision, Sweden) staining protocol. This protocol produces
798 purple hues typical of Romanowsky-Giemsa staining results. After staining, the samples were
799 observed using a LEICA DMR (Leica AG, Germany) transmitted light microscope with a 40x
800 magnification objective. Each slide was imaged and the hemocytes were counted and
801 characterized based on their morphology.

802 **Real Time-quantitative Polymerase Chain Reaction (RT-qPCR)**

803 Total RNA was extracted using the RNeasy kit (Qiagen, the Netherlands) and cDNA was
804 synthesized from 1 µg total RNA using the Superscript IV kit (ThermoFisher Scientific, USA)
805 with oligo(dT) primers. RT-PCR was performed on LightCycler© 480 thermocycler using the
806 SYBR Green 1 Master kit (Roche, Switzerland). Primers were used at 200 nM. Primer sequences
807 are listed in **Supplementary Table S3**. Expression was normalized to *Cg-rps6* reference gene.
808 The standard cycling conditions were 95°C pre-incubation for 3 minutes followed by 40 cycles of
809 95°C for 10 seconds, 60°C for 20 seconds, and 72°C for 25 seconds. Each pair of primers was
810 first tested and validated on a total hemocyte RNA preparation to control melting curves and
811 establish calibration lines.

812 **Oxidative Burst Assay**

813 The production of reactive oxygen species was quantified by luminescence assay. Briefly,
814 hemocytes from hemolymph puncture or Percoll density gradient were washed once with filtered
815 sterile water. 50 µL of hemocytes were plated in triplicate on a 96-well plate (3.10^5 cells/cm²). 50
816 µL of 40 mM luminol (Merck and Co, USA) was added to each well. After 45 minutes of

817 incubation at room temperature, the oxidative burst was induced by adding 100 µL of zymosan
818 (Merck and Co, USA) at a multiplicity of infection (MOI) of 50:1. The plate was immediately
819 placed in a luminescence microplate reader Berthold Centro XS3 LB 960 (Berthold GmbH,
820 Germany) to measure luminescence emission every 2 minutes for 2 hours.

821 **Phagocytosis assay**

822 400 µL of filtered, sterile water-washed hemocytes were seeded in a 24-well plate at a
823 concentration of 3.10^5 cells/cm². After 15 minutes, 50 µL of zymosan was added to the fractions
824 at a MOI of 20:1. For LMG20012t Vibrio, 50 µL of bacteria was added to a total hemolymph at a
825 MOI of 5:1. After 1 hour of contact at room temperature, the cells were resuspended and 200 µL
826 of the suspension was applied to a microscope slide using a Cytospin centrifuge. The slides were
827 then stained with MCDH and observed under a transmitted light microscope LEICA DMR with
828 40x magnification objective (Leica AG, Germany) to count phagocytic cells.

829 **NitroBlueTetrazolium (NBT) staining**

830 The production of reactive oxygen species was measured using NitroBlue Tetrazolium reduction
831 after zymosan stimulation. Briefly, 1 mL (1.10^6 cells) of hemocyte solution was mixed with 50 µL
832 of filtered NBT solution (15 mg/mL in water). Zymosan was added at a 4:1 MOI and the mixture
833 was incubated at room temperature for 10 minutes on a rocking shaker, then 50 µL of each
834 sample was plated onto glass coverslips and observed under a transmitted light microscope
835 LEICA DMR with 40x magnification objective (Leica AG, Germany) to count NBT-positive
836 cells. The positions of positive NBT cells were recorded prior to MCDH staining to identify
837 hemocyte types.

838 **Rhodanine copper staining of hemocytes**

839 The storage of copper by hemocytes was examined by Rhodanine staining. Briefly, 1.10^5
840 hemocytes were plated on Superfrost slides using a cytospin and circled with a hydrophobic pen
841 to retain the staining solution. The Copper Stain Kit (SkyTek, USA) was used to stain the

842 hemocytes. As described by the kit manufacturer, one drop of Rhodanine solution was added to 9
843 drops of acetate to form the working solution. Five drops were placed on the cytospin cells and a
844 5 mL Eppendorf tube with the cap removed was placed over the cells to prevent evaporation of
845 the working solution. The slide and the balanced Eppendorf tube were placed on a beaker of
846 boiling distilled water for 20 minutes. The slide was then washed with 5 drops of acetate and 3
847 drops of hematoxylin were placed on the slide for 1 minute at room temperature. The slides were
848 then washed a final time with acetate and observed under a LEICA DMR transmitted light
849 microscope with a 40x magnification objective (Leica AG, Germany) to count rhodanine-positive
850 cells. The positions of rhodanine-positive cells were recorded prior to MCDH staining to identify
851 hemocyte types.

852 **Pseudotemporal ordering of cells with Monocle3**

853 Cells from the *C. gigas* dataset were analyzed using Monocle3 (https://github.com/cole-trapnell-
854 lab/monocle3) (*39*). The Monocle3 analysis was performed on the Seurat object after processing
855 described above. Clustering information (features, genes, partitions, clusters and UMAP
856 coordinates) was transferred to a CDS object. The cell trajectory was calculated using the
857 *learn_graph* function. Three lineages were selected by using *choose_graph_segments* function.
858 The gene expression along pseudotime data was extracted from the result. Then the data were
859 used to plot genes along pseudotime in three lineages using ggplot2 v3.4.4 R package and the
860 heatmap was generated using pheatmap v1.0.12 R package.

861 **Statistical Analysis**

862 To assess differences between samples, statistical analysis was performed using (version 4.2.1) (R
863 Core Team, 2018) and appropriate packages. All data were examined for normality, and statistical
864 tests were chosen accordingly. For normally distributed data, one-way analysis of variance
865 (ANOVA) was used. For cytological analysis, 7 different hemolymph samples were used. Oysters
866 were provided by our local supplier) and approximately 300 hemocytes were counted per sample.

867 For Percoll density gradient separation, 7 independent experiments were performed. A Tukey test
868 was used to evaluate the statistical difference between the proportions of hemocyte types. The
869 phagocytic capacity of hemocytes was tested in three independent experiments and statistical
870 differences were evaluated using the Tukey test for both the phagocytic capacity between
871 hemocyte types and the number of particles per phagocyte. Finally, oxidative burst capacity was
872 tested 3 times on Percoll-separated hemocytes. The Tukey test was also used to assess statistical
873 differences between conditions. The null hypothesis was rejected at a significance level of $p =$
874 0.05.

875 **References**

876

877 1. Y. M. Bar-On, R. Phillips, R. Milo, The biomass distribution on Earth. *Proc. Natl. Acad. Sci.* **115**, 6506–6511
878 (2018).
879 2. B. Leicester Bayne, *Biology of Oysters* (Academic Press, 1st Edition., 2017)vol. 41.
880 3. G. Zhang, L. Li, J. Meng, H. Qi, T. Qu, F. Xu, L. Zhang, Molecular Basis for Adaptation of Oysters to Stressful
881 Marine Intertidal Environments. *Annu. Rev. Anim. Biosci.* **4**, 357–381 (2016).
882 4. FAO, Global aquaculture production. Fisheries and aquaculture division (2023).
883 5. F. Pernet, C. Lupo, C. Bacher, R. J. Whittington, Infectious diseases in oyster aquaculture require a new
884 integrated approach. *Philos. Trans. R. Soc. B Biol. Sci.* **371**, 20150213 (2016).
885 6. A. Alfjorden, M. Areskog, D. Bruno, R. Carnegie, D. Cheslett, S. Feist, S. Ford, S. Jones, A. Lillehaug, L.
886 Madsen, T. Renault, N. Ruane, P. Vennerstrom, New Trends in Important Diseases Affecting the Culture of Fish
887 and Molluscs in the ICES Area 2002– 2015. *ICES Coop. Res. Rep.*, doi: 10.17895/ices.pub.2800 (2017).
888 7. J. de Lorgeril, A. Lucasson, B. Petton, E. Toulza, C. Montagnani, C. Clerissi, J. Vidal-Dupiol, C. Chaparro, R.
889 Galinier, J.-M. Escoubas, P. Haffner, L. Dégremont, G. M. Charrière, M. Lafont, A. Delort, A. Vergnes, M.
890 Chiarello, N. Faury, T. Rubio, M. A. Leroy, A. Pérignon, D. Régler, B. Morga, M. Alunno-Bruscia, P. Boudry,
891 F. Le Roux, D. Destoumieux-Garzón, Y. Gueguen, G. Mitta, Immune-suppression by OsHV-1 viral infection
892 causes fatal bacteraemia in Pacific oysters. *Nat. Commun.* **9**, 4215 (2018).
893 8. N. M. Coyle, C. O'Toole, J. C. L. Thomas, D. Ryder, E. J. Feil, M. Geary, T. P. Bean, A. W. Joseph, A. Waine,
894 D. Cheslett, D. W. Verner-Jeffreys, Vibrio aestuarianus Clade A and Clade B isolates are associated with Pacific
895 oyster (Crassostrea gigas) disease outbreaks across Ireland. bioRxiv [Preprint] (2023).
896 https://doi.org/10.1101/2023.04.06.535062.
897 9. A. Mesnil, M. Jacquot, C. Garcia, D. Tourbiez, L. Canier, A. Bidois, L. Dégremont, D. Cheslett, M. Geary, A.
898 Vetri, A. Roque, D. Furones, A. Garden, P. Orozova, I. Arzul, M. Sicard, G. M. Charrière, D. Destoumieux-
899 Garzón, M.-A. Travers, Emergence and clonal expansion of Vibrio aestuarianus lineages pathogenic for oysters
900 in Europe. *Mol. Ecol.* **32**, 2869–2883 (2023).
901 10. D. Oyanedel, A. Lagorce, M. Bruto, P. Haffner, A. Morot, Y. Labreuche, Y. Dorant, S. de La Forest Divonne, F.
902 Delavat, N. Inguimbert, C. Montagnani, B. Morga, E. Toulza, C. Chaparro, J.-M. Escoubas, Y. Gueguen, J.
903 Vidal-Dupiol, J. de Lorgeril, B. Petton, L. Degremont, D. Tourbiez, L.-L. Pimparé, M. Leroy, O. Romatif, J.
904 Pouzadoux, G. Mitta, F. Le Roux, G. M. Charrière, M.-A. Travers, D. Destoumieux-Garzón, Cooperation and
905 cheating orchestrate Vibrio assemblages and polymicrobial synergy in oysters infected with OsHV-1 virus.
906 *Proc. Natl. Acad. Sci.* **120**, e2305195120 (2023).
907 11. T. Rubio, D. Oyanedel, Y. Labreuche, E. Toulza, X. Luo, M. Bruto, C. Chaparro, M. Torres, J. de Lorgeril, P.
908 Haffner, J. Vidal-Dupiol, A. Lagorce, B. Petton, G. Mitta, A. Jacq, F. Le Roux, G. M. Charrière, D.
909 Destoumieux-Garzón, Species-specific mechanisms of cytotoxicity toward immune cells determine the
910 successful outcome of Vibrio infections. *Proc. Natl. Acad. Sci.* **116**, 14238–14247 (2019).
911 12. Y. Labreuche, F. Le Roux, J. Henry, C. Zatylny, A. Huvet, C. Lambert, P. Soudant, D. Mazel, J.-L. Nicolas,
912 Vibrio aestuarianus zinc metalloprotease causes lethality in the Pacific oyster Crassostrea gigas and impairs the
913 host cellular immune defenses. *Fish Shellfish Immunol.* **29**, 753–758 (2010).
914 13. M. Lafont, A. Vergnes, J. Vidal-Dupiol, J. de Lorgeril, Y. Gueguen, P. Haffner, B. Petton, C. Chaparro, C.
915 Barrachina, D. Destoumieux-Garzon, G. Mitta, B. Gourbal, C. Montagnani, A Sustained Immune Response

Supports Long-Term Antiviral Immune Priming in the Pacific Oyster, Crassostrea gigas. *mBio* **11**, 10.1128/mbio.02777-19 (2020).
14. M. Fallet, C. Montagnani, B. Petton, L. Dantan, J. de Lorgeril, S. Comarmond, C. Chaparro, E. Toulza, S. Boitard, J.-M. Escoubas, A. Vergnes, J. Le Grand, I. Bulla, Y. Gueguen, J. Vidal-Dupiol, C. Grunau, G. Mitta, C. Cosseau, Early life microbial exposures shape the Crassostrea gigas immune system for lifelong and intergenerational disease protection. *Microbiome* **10**, 85 (2022).
15. N. R. de la Ballina, F. Maresca, A. Cao, A. Villalba, Bivalve Haemocyte Subpopulations: A Review. *Front. Immunol.* **13** (2022).
16. E. Bachère, R. D. Rosa, P. Schmitt, A. C. Poirier, N. Merou, G. M. Charrière, D. Destoumieux-Garzón, The new insights into the oyster antimicrobial defense: Cellular, molecular and genetic view. *Fish Shellfish Immunol.* **46**, 50–64 (2015).
17. J.-M. Escoubas, B. Gourbal, D. Duval, T. J. Green, G. M. Charrière, D. Destoumieux-Garzón, C. Montagnani, "Immunity in Molluscs" in *Encyclopedia of Immunobiology*, M. J. H. Ratcliffe, Ed. (Academic Press, Oxford, 2016; https://www.sciencedirect.com/science/article/pii/B9780123742797120041), pp. 417–436.
18. A. S. Mount, A. P. Wheeler, R. P. Paradkar, D. Snider, Hemocyte-Mediated Shell Mineralization in the Eastern Oyster. *Science*, doi: 10.1126/science.1090506 (2004).
19. W. S. FısıER, "Environmental influence on bivalve hemocyte function" in *Am Fish Soc Symp* (1988; https://www.researchgate.net/profile/William-Fisher-29/publication/285361443_Environmental_influence_on_bivalve_hemocyte_function/links/5d435d5f299bf1995b5e5d4c/Environmental-influence-on-bivalve-hemocyte-function.pdf)vol. 18, pp. 225–237.
20. T. V. Nguyen, A. C. Alfaro, F. Merien, Omics approaches to investigate host–pathogen interactions in mass mortality outbreaks of Crassostrea gigas. *Rev. Aquac.* **11**, 1308–1324 (2019).
21. J. Meng, G. Zhang, W.-X. Wang, Functional heterogeneity of immune defenses in molluscan oysters Crassostrea hongkongensis revealed by high-throughput single-cell transcriptome. *Fish Shellfish Immunol.* **120**, 202–213 (2022).
22. R. D. Rosa, P. Alonso, A. Santini, A. Vergnes, E. Bachère, High polymorphism in big defensin gene expression reveals presence–absence gene variability (PAV) in the oyster Crassostrea gigas. *Dev. Comp. Immunol.* **49**, 231–238 (2015).
23. B. Kaminow, D. Yunusov, A. Dobin, STARsolo: accurate, fast and versatile mapping/quantification of single-cell and single-nucleus RNA-seq data. bioRxiv [Preprint] (2021). https://doi.org/10.1101/2021.05.05.442755.
24. C. Peñaloza, A. P. Gutierrez, L. Eöry, S. Wang, X. Guo, A. L. Archibald, T. P. Bean, R. D. Houston, A chromosome-level genome assembly for the Pacific oyster Crassostrea gigas. *GigaScience* **10**, giab020 (2021).
25. R. Satija, J. A. Farrell, D. Gennert, A. F. Schier, A. Regev, Spatial reconstruction of single-cell gene expression data. *Nat. Biotechnol.* **33**, 495–502 (2015).
26. B. T. Sherman, M. Hao, J. Qiu, X. Jiao, M. W. Baseler, H. C. Lane, T. Imamichi, W. Chang, DAVID: a web server for functional enrichment analysis and functional annotation of gene lists (2021 update). *Nucleic Acids Res.* **50**, W216–W221 (2022).
27. C. Peñaloza, A. P. Gutierrez, L. Eöry, S. Wang, X. Guo, A. L. Archibald, T. P. Bean, R. D. Houston, A chromosome-level genome assembly for the Pacific oyster Crassostrea gigas. *GigaScience* **10**, giab020 (2021).
28. R. M. Wright, G. V. Aglyamova, E. Meyer, M. V. Matz, Gene expression associated with white syndromes in a reef building coral, Acropora hyacinthus. *BMC Genomics* **16**, 371 (2015).
29. E. Bachère, D. Chagot, H. Grizel, Separation of Crassostrea gigas hemocytes by density gradient centrifugation and counterflow centrifugal elutriation. *Dev. Comp. Immunol.* **12**, 549–559 (1988).
30. W. Wang, M. Li, L. Wang, H. Chen, Z. Liu, Z. Jia, L. Qiu, L. Song, The granulocytes are the main immunocompetent hemocytes in Crassostrea gigas. *Dev. Comp. Immunol.* **67**, 221–228 (2017).
31. C. Lambert, P. Soudant, G. Choquet, C. Paillard, Measurement of Crassostrea gigas hemocyte oxidative metabolism by flow cytometry and the inhibiting capacity of pathogenic vibrios. *Fish Shellfish Immunol.* **15**, 225–240 (2003).
32. A. Mesnil, M. Jacquot, C. Garcia, D. Tourbiez, L. Canier, A. Bidois, L. Dégremont, D. Cheslett, M. Geary, A. Vetri, A. Roque, D. Furones, A. Garden, P. Orozova, I. Arzul, M. Sicard, G. M. Charrière, D. Destoumieux-Garzón, M.-A. Travers, Emergence and clonal expansion of Vibrio aestuarianus lineages pathogenic for oysters in Europe. *Mol. Ecol.* **32**, 2869–2883 (2023).
33. P. Schmitt, R. Rosa, M. Duperthuy, J. de Lorgeril, E. Bachère, D. Destoumieux-Garzon, The Antimicrobial Defense of the Pacific Oyster, Crassostrea gigas. How Diversity may Compensate for Scarcity in the Regulation of Resident/Pathogenic Microflora. *Front. Microbiol.* **3** (2012).
34. G. Vogt, Hidden Treasures in Stem Cells of Indeterminately Growing Bilaterian Invertebrates. *Stem Cell Rev. Rep.* **8**, 305–317 (2012).
35. M. Jemaà, N. Morin, P. Cavelier, J. Cau, J. M. Strub, C. Delsert, Adult somatic progenitor cells and hematopoiesis in oysters. *J. Exp. Biol.* **217**, 3067–3077 (2014).
36. S. P. Fahl, M. Wang, Y. Zhang, A.-C. E. Duc, D. L. Wiest, Regulatory Roles of Rpl22 in Hematopoiesis: An

Old Dog with New Tricks. *Crit. Rev. Immunol.* **35**, 379–400 (2015).
37. L. Jarzebowski, M. Le Bouteiller, S. Coqueran, A. Raveux, S. Vandormael-Pournin, A. David, A. Cumano, M. Cohen-Tannoudji, Mouse adult hematopoietic stem cells actively synthesize ribosomal RNA. *RNA* **24**, 1803–1812 (2018).
38. M. Rehn, A. Wenzel, A.-K. Frank, M. B. Schuster, S. Pundhir, N. Jørgensen, K. Vitting-Seerup, Y. Ge, J. Jendholm, M. Michaut, E. M. Schoof, T. L. Jensen, N. Rapin, R. T. Sapio, K. L. Andersen, A. H. Lund, M. Solimena, M. Holzenberger, D. G. Pestov, B. T. Porse, PTBP1 promotes hematopoietic stem cell maintenance and red blood cell development by ensuring sufficient availability of ribosomal constituents. *Cell Rep.* **39**, 110793 (2022).
39. J. Cao, M. Spielmann, X. Qiu, X. Huang, D. M. Ibrahim, A. J. Hill, F. Zhang, S. Mundlos, L. Christiansen, F. J. Steemers, C. Trapnell, J. Shendure, The single-cell transcriptional landscape of mammalian organogenesis. *Nature* **566**, 496–502 (2019).
40. D. Hultmark, I. Andó, Hematopoietic plasticity mapped in Drosophila and other insects. *eLife* **11**, e78906 (2022).
41. U. Banerjee, J. R. Girard, L. M. Goins, C. M. Spratford, Drosophila as a Genetic Model for Hematopoiesis. *Genetics* **211**, 367–417 (2019).
42. E. Boada-Romero, J. Martinez, B. L. Heckmann, D. R. Green, The clearance of dead cells by efferocytosis. *Nat. Rev. Mol. Cell Biol.* **21**, 398–414 (2020).
43. D. C. Dale, L. Boxer, W. C. Liles, The phagocytes: neutrophils and monocytes. *Blood* **112**, 935–945 (2008).
44. T. Rubio, D. Oyanedel, Y. Labreuche, E. Toulza, X. Luo, M. Bruto, C. Chaparro, M. Torres, J. de Lorgeril, P. Haffner, J. Vidal-Dupiol, A. Lagorce, B. Petton, G. Mitta, A. Jacq, F. Le Roux, G. M. Charrière, D. Destoumieux-Garzón, Species-specific mechanisms of cytotoxicity toward immune cells determine the successful outcome of Vibrio infections. *Proc. Natl. Acad. Sci.* **116**, 14238–14247 (2019).
45. A. S. Vanhove, T. P. Rubio, A. N. Nguyen, A. Lemire, D. Roche, J. Nicod, A. Vergnes, A. C. Poirier, E. Disconzi, E. Bachère, F. Le Roux, A. Jacq, G. M. Charrière, D. Destoumieux-Garzón, Copper homeostasis at the host vibrio interface: lessons from intracellular vibrio transcriptomics. *Environ. Microbiol.* **18**, 875–888 (2016).
46. A. C. Poirier, P. Schmitt, R. D. Rosa, A. S. Vanhove, S. Kieffer-Jaquinod, T. P. Rubio, G. M. Charrière, D. Destoumieux-Garzón, Antimicrobial Histones and DNA Traps in Invertebrate Immunity. *J. Biol. Chem.* **289**, 24821–24831 (2014).
47. A. C. Poirier, P. Schmitt, R. D. Rosa, A. S. Vanhove, S. Kieffer-Jaquinod, T. P. Rubio, G. M. Charrière, D. Destoumieux-Garzón, Antimicrobial Histones and DNA Traps in Invertebrate Immunity: Evidences in Crassostrea Gigas *. *J. Biol. Chem.* **289**, 24821–24831 (2014).
48. G. Zaroogian, P. Yevich, Cytology and biochemistry of brown cells in *Crassostrea virginica* collected at clean and contaminated stations. *Environ. Pollut.* **79**, 191–197 (1993).
49. B. Allam, D. Raftos, Immune responses to infectious diseases in bivalves. *J. Invertebr. Pathol.* **131**, 121–136 (2015).
50. J. Nakhleh, L. El Moussawi, M. A. Osta, "Chapter Three - The Melanization Response in Insect Immunity" in *Advances in Insect Physiology*, P. Ligoxygakis, Ed. (Academic Press, 2017; https://www.sciencedirect.com/science/article/pii/S0065280616300467)vol. 52 of *Insect Immunity*, pp. 83–109.
51. P. Amparyup, W. Charoensapsri, A. Tassanakajon, Prophenoloxidase system and its role in shrimp immune responses against major pathogens. *Fish Shellfish Immunol.* **34**, 990–1001 (2013).
52. S. Picot, N. Faury, C. Pelletier, I. Arzul, B. Chollet, L. Dégremont, T. Renault, B. Morga, Monitoring Autophagy at Cellular and Molecular Level in Crassostrea gigas During an Experimental Ostreid Herpesvirus 1 (OsHV-1) Infection. *Front. Cell. Infect. Microbiol.* **12** (2022).
53. N. R. de la Ballina, A. Villalba, A. Cao, Differences in proteomic profile between two haemocyte types, granulocytes and hyalinocytes, of the flat oyster *Ostrea edulis*. *Fish Shellfish Immunol.* **100**, 456–466 (2020).
54. S. Aladaileh, S. V. Nair, D. Birch, D. A. Raftos, Sydney rock oyster (*Saccostrea glomerata*) hemocytes: Morphology and function. *J. Invertebr. Pathol.* **96**, 48–63 (2007).
55. E. Rifkin, T. C. Cheng, H. R. Hohl, An electron-microscope study of the constituents of encapsulating cysts in the American oyster, *Crassostrea virginica*, formed in response to *Tylocephalum* metacestodes. *J. Invertebr. Pathol.* **14**, 211–226 (1969).
56. N. De San Nicolas, A. Asokan, R. D. Rosa, S. N. Voisin, M.-A. Travers, G. Rocha, L. Dantan, Y. Dorant, G. Mitta, B. Petton, G. M. Charrière, J.-M. Escoubas, V. Boulo, J. Pouzadoux, H. Meudal, K. Loth, V. Aucagne, A. F. Delmas, P. Bulet, C. Montagnani, D. Destoumieux-Garzón, Functional Diversification of Oyster Big Defensins Generates Antimicrobial Specificity and Synergy against Members of the Microbiota. *Mar. Drugs* **20**, 745 (2022).
57. N. R. de la Ballina, A. Villalba, A. Cao, Shotgun analysis to identify differences in protein expression between granulocytes and hyalinocytes of the European flat oyster Ostrea edulis. *Fish Shellfish Immunol.* **119**, 678–691 (2021).
58. J. de Lorgeril, A. Lucasson, B. Petton, E. Toulza, C. Montagnani, C. Clerissi, J. Vidal-Dupiol, C. Chaparro, R.

Galinier, J.-M. Escoubas, P. Haffner, L. Dégremont, G. M. Charrière, M. Lafont, A. Delort, A. Vergnes, M. Chiarello, N. Faury, T. Rubio, M. A. Leroy, A. Pérignon, D. Régler, B. Morga, M. Alunno-Bruscia, P. Boudry, F. Le Roux, D. Destoumieux-Garzón, Y. Gueguen, G. Mitta, Immune-suppression by OsHV-1 viral infection causes fatal bacteraemia in Pacific oysters. *Nat. Commun.* **9**, 4215 (2018).

59. E. A. Pila, J. T. Sullivan, X. Z. Wu, J. Fang, S. P. Rudko, M. A. Gordy, P. C. Hanington, Haematopoiesis in molluscs: A review of haemocyte development and function in gastropods, cephalopods and bivalves. *Dev. Comp. Immunol.* **58**, 119–128 (2016).
60. M. de Bruijn, E. Dzierzak, Runx transcription factors in the development and function of the definitive hematopoietic system. *Blood* **129**, 2061–2069 (2017).
61. E. W. Scott, M. C. Simon, J. Anastasi, H. Singh, Requirement of transcription factor PU.1 in the development of multiple hematopoietic lineages. *Science* **265**, 1573–1577 (1994).
62. I. Bergiers, T. Andrews, Ö. Vargel Bölükbaşı, A. Buness, E. Janosz, N. Lopez-Anguita, K. Ganter, K. Kosim, C. Celen, G. Itır Perçin, P. Collier, B. Baying, V. Benes, M. Hemberg, C. Lancrin, Single-cell transcriptomics reveals a new dynamical function of transcription factors during embryonic hematopoiesis. *eLife* **7**, e29312 (2018).
63. S. F. Altschul, W. Gish, W. Miller, E. W. Myers, D. J. Lipman, Basic local alignment search tool. *J. Mol. Biol.* **215**, 403–410 (1990).
64. P. Jones, D. Binns, H.-Y. Chang, M. Fraser, W. Li, C. McAnulla, H. McWilliam, J. Maslen, A. Mitchell, G. Nuka, S. Pesseat, A. F. Quinn, A. Sangrador-Vegas, M. Scheremetjew, S.-Y. Yong, R. Lopez, S. Hunter, InterProScan 5: genome-scale protein function classification. *Bioinformatics* **30**, 1236–1240 (2014).
65. C. P. Cantalapiedra, A. Hernández-Plaza, I. Letunic, P. Bork, J. Huerta-Cepas, eggNOG-mapper v2: Functional Annotation, Orthology Assignments, and Domain Prediction at the Metagenomic Scale. *Mol. Biol. Evol.* **38**, 5825–5829 (2021).
66. S. Götz, J. M. García-Gómez, J. Terol, T. D. Williams, S. H. Nagaraj, M. J. Nueda, M. Robles, M. Talón, J. Dopazo, A. Conesa, High-throughput functional annotation and data mining with the Blast2GO suite. *Nucleic Acids Res.* **36**, 3420–3435 (2008).
67. Y. Hao, S. Hao, E. Andersen-Nissen, W. M. Mauck, S. Zheng, A. Butler, M. J. Lee, A. J. Wilk, C. Darby, M. Zager, P. Hoffman, M. Stoeckius, E. Papalexi, E. P. Mimitou, J. Jain, A. Srivastava, T. Stuart, L. M. Fleming, B. Yeung, A. J. Rogers, J. M. McElrath, C. A. Blish, R. Gottardo, P. Smibert, R. Satija, Integrated analysis of multimodal single-cell data. *Cell* **184**, 3573-3587.e29 (2021).
68. R. M. Wright, G. V. Aglyamova, E. Meyer, M. V. Matz, Gene expression associated with white syndromes in a reef building coral, Acropora hyacinthus. *BMC Genomics* **16**, 371 (2015).

Acknowledgments

We are grateful to the staff of the Ifremer platform of "La Tremblade" for technical support in animal housing. scRNA-seq data generated and used in this work were produced through the MGX platform (University of Montpellier, CNRS ,INSERM). We thank the bioinformatic service of Ifremer (SEBIMER) for their help in bioinformatics and the qPCR platform GenSeq (University of Montpellier). We would like to thank Viviane Boulo and Danielle Mello for their enriching discussions, as well as all the members of the 2MAP laboratory team for the fruitful discussions throughout this project.

Ethics

This work did not require ethical approval from a human subject or animal welfare committee.

Funding

This work was funded by the Agence Nationale de la Recherche (MOSAR-DEF, ANR-19-CE18-0025; DECICOMP, ANR-19-CE20-0004 and TRANSCAN ANR-18-CE35-0009), the University of Montpellier, iSite MUSE and the "GT-Huître" initiative from Ifremer. This study falls within the framework of the "Laboratoires d'Excellence (LABEX)" Tulip (ANR-10-LABX-41). Sébastien De La Forest Divonne was awarded a PhD grant from the Region Occitanie (HemoFight project) and the University of Perpignan Via Domitia graduate school ED305.

Author contributions

Conceptualization: G.M., D.D.-G., B.G., G.M.C. and E.V.

Methodology: S.d.L.F.D., J.P., G.M., D.D.-G., B.G., G.M.C. and E.V.

Investigation: S.d.L.F.D., J.P., G.M.C. and E.V.

Supervision: G.M.C. and E.V.

Writing (original draft): S.d.L.F.D. and E.V.

Writing (review and editing): all authors.

Competing interests

The authors declare that they have no competing interests.